

# 1 Reconstruction of the 1941 GLOF process chain at Lake Palcacocha (Cordillera Blanca, Perú)

3 ***Martin Mergili<sup>1,2</sup>, Shiva P. Pudasaini<sup>3</sup>, Adam Emmer<sup>4</sup>, Jan-Thomas Fischer<sup>5</sup>,  
4 Alejo Cochachin<sup>6</sup>, and Holger Frey<sup>7</sup>***

5 <sup>1</sup> Institute of Applied Geology, University of Natural Resources and Life Sciences (BOKU), Peter-Jordan-  
6 Straße 82, 1190 Vienna, Austria

7 <sup>2</sup> Geomorphological Systems and Risk Research, Department of Geography and Regional Research, Uni-  
8 versity of Vienna, Universitätsstraße 7, 1010 Vienna, Austria

9 <sup>3</sup> Geophysics Section, Institute of Geosciences, University of Bonn, Meckenheimer Allee 176, 53115  
10 Bonn, Germany

11 <sup>4</sup> Department of the Human Dimensions of Global Change, Global Change Research Institute, The Czech  
12 Academy of Sciences, Bělidla 986/4a, 603 00, Brno, Czech Republic

13 <sup>5</sup> Department of Natural Hazards, Austrian Research Centre for Forests (BFW), Rennweg 1, 6020 Inns-  
14 bruck, Austria

15 <sup>6</sup> Unidad de Glaciología y Recursos Hídricos, Autoridad Nacional del Agua, Confraternidad Internacional  
16 167, Huaráz, Perú

17 <sup>7</sup> Department of Geography, University of Zurich, Winterthurerstrasse 190, 8057 Zurich, Switzerland

18 Correspondence to: M. Mergili (martin.mergili@boku.ac.at)

## 19 **Abstract**

20 The Cordillera Blanca in Perú has been the scene of rapid deglaciation for many decades. One of numer-  
21 ous lakes formed in the front of the retreating glaciers is the moraine-dammed Lake Palcacocha, which  
22 drained suddenly due to an unknown cause in 1941. The resulting Glacial Lake Outburst Flood (GLOF)  
23 led to dam failure and complete drainage of Lake Jircacocha downstream, and to major destruction and  
24 thousands of fatalities in the city of Huaráz at a distance of 23 km. We chose an integrated approach to  
25 revisit the 1941 event in terms of topographic reconstruction and numerical back-calculation with the  
26 GIS-based open source mass flow/process chain simulation framework *r.avaflood*, which builds on an  
27 enhanced version of the Pudasaini (2012) two-phase flow model. Thereby we consider four scenarios:  
28 (A) and (AX) breach of the moraine dam of Lake Palcacocha due to retrogressive erosion, assuming two  
29 different fluid characteristics; (B) failure of the moraine dam caused by the impact of a landslide onto the  
30 lake; and (C) geomechanical failure and collapse of the moraine dam. The simulations largely yield em-  
31 pirically adequate results with physically plausible parameters, taking the documentation of the 1941  
32 event and previous calculations of future scenarios as reference. Most simulation scenarios indicate trav-  
33 el times between 36 and 70 minutes to reach Huaráz, accompanied with peak discharges above 10,000  
34 m<sup>3</sup>/s. The results of the scenarios indicate that the most likely initiation mechanism would be retrogres-  
35 sive erosion, possibly triggered by a minor impact wave and/or facilitated by a weak stability condition

36 of the moraine dam. However, the involvement of Lake Jircacocha disguises part of the signal of process  
37 initiation farther downstream. Predictive simulations of possible future events have to be based on a  
38 larger set of back-calculated GLOF process chains, taking into account the expected parameter uncer-  
39 tainties and appropriate strategies to deal with critical threshold effects.

40 **Keywords:** GLOF, high-mountain lakes, Lake Palcacocha, numerical simulation, process chain,  
41 ravaflow, two-phase flows

## 42 **1 Introduction**

43 Glacial retreat in high-mountain areas often leads, after some lag time (Harrison et al., 2018), to the for-  
44 mation of proglacial lakes, which are impounded by moraine dams or bedrock swells. Such lakes may  
45 drain suddenly, releasing a large amount of water which may result in complex and potentially cata-  
46 strophic process chains downstream. Glacial lakes and outburst floods (GLOFs) have been subject of nu-  
47 merous studies covering many mountain regions all around the globe (Hewitt, 1982; Haeberli, 1983;  
48 Richardson and Reynolds, 2000; Huggel et al., 2003; Breien et al., 2008; Hewitt and Liu, 2010;  
49 Bolch et al., 2011; Mergili and Schneider, 2011; Mergili et al., 2013; Clague and O'Connor, 2014; Em-  
50 mer et al., 2015, 2016; Sattar et al., 2019a, b; Turzewski et al., 2019).

51 The Cordillera Blanca (Perú) represents the most glacierized mountain chain of the Tropics. Glacial lakes  
52 and GLOFs are particularly common there (Carey, 2005). 882 high-mountain lakes were identified by  
53 Emmer et al. (2016). Some of these lakes are susceptible to GLOFs (Vilímek et al., 2005; Em-  
54 mer and Vilímek, 2013, 2014; ANA, 2014; Iturriaga, 2014). A total of 28 geomorphologically effective  
55 GLOFs originating from moraine-dammed lakes have been documented (Emmer, 2017). Most recently,  
56 GLOFs were recorded at Lake Safuna Alta (2002 – the trigger was a rock avalanche into the lake; Hub-  
57 bard et al., 2005), at Lake Palcacocha (2003 – landslide-induced overtopping of the dam; Vilímek et al.,  
58 2005), and at Lake 513 (2010 – triggered by an ice avalanche; Carey et al., 2012). Lake Artizón Alto was  
59 hit by a landslide from a moraine in 2012, which resulted in cascading effects involving three more lakes  
60 and entrainment of a considerable amount of debris in the Artizón Valley and, farther downstream, the  
61 Santa Cruz Valley (Mergili et al., 2018a). A pronounced peak in frequency of high-magnitude GLOFs,  
62 however, was already observed in the 1940s and 1950s, when lakes of notable size had formed behind  
63 steep terminal moraine walls (Emmer et al., 2019). The most prominent and well-documented GLOF in  
64 this period occurred on 13 December 1941, when Lake Palcacocha in the Quilcay Catchment drained  
65 suddenly, leading to a process chain that resulted in at least 1600 fatalities and major destruction in the  
66 town of Huaráz 23 km downstream (Broggi, 1942; Oppenheim, 1946; Concha, 1952; Wegner, 2014).

67 In the Cordillera Blanca, the local population is highly vulnerable to high-mountain process chains, of-  
68 ten induced by GLOFs (Carey, 2005; Hofflinger et al., 2019). In order to mitigate this threat, tens of lakes  
69 in the Cordillera Blanca have been remediated through technical measures such as open cuts, artificial  
70 dams or tunnels during the last decades (Oppenheim, 1946; Zapata 1978; Portocarrero, 1984; Carey,  
71 2005; Portocarrero, 2014; Emmer et al., 2018). Most notably, lowering the lake level of Laguna 513  
72 through a system of tunnels in the 1990s has probably prevented a disaster downstream when a rock-ice  
73 avalanche impacted that lake in 2010 (Reynolds, 1998; Reynolds et al., 1998; Schneider et al., 2014).  
74 However, the management of GLOF risk is a difficult task (Carey et al., 2014). Anticipation of the impact

75 area and magnitude of GLOF cascades – and, as a consequence, also hazard mapping and the design of  
76 technical remediation measures – relies to a large extent on the application of computational mass flow  
77 models (GAPHAZ, 2017). Important progress was made since the mid-20<sup>th</sup> Century: various models were  
78 developed, and have more recently been implemented in simulation software tools (Voellmy, 1955; Sav-  
79 age and Hutter, 1989; Iverson, 1997; Takahashi et al., 2002; Pitman and Le, 2005; McDougall and Hungr,  
80 2004; Pudasaini and Hutter, 2007; Chisolm and McKinney, 2018). Most of these approaches represent  
81 single-phase mixture models. Tools like RAMMS (Christen et al., 2010) or FLO-2D were used for the  
82 simulation of GLOFs (Mergili et al., 2011). Schneider et al. (2014), Worni et al. (2014), and Somos-  
83 Valenzuela et al. (2016) have sequentially coupled two or more tools for simulating landslide – GLOF  
84 cascades. However, single-phase models do not describe the interactions between the solid and the fluid  
85 phase, or dynamic landslide-lake interactions, in an appropriate way, so that workarounds are necessary  
86 (Gabl et al., 2015). Worni et al. (2014) called for integrated approaches. They would have to build on  
87 two- or even three-phase models considering water, debris, and ice separately, but also the interactions  
88 between the phases and the flow transformations. Pudasaini (2012) introduced a general two-phase flow  
89 model considering mixtures of solid particles and viscous fluid which has been used for the simulation of  
90 computer-generated examples of sub-aqueous landslides and particle transport (Kafle et al., 2016, 2019)  
91 as well as GLOFs (Kattel et al., 2016).

92 The recently introduced open source GIS simulation framework r.avaflow (Mergili et al., 2017) applies  
93 an extended version of the approach of Pudasaini (2012). It was used to back-calculate the 2012 Santa  
94 Cruz process chain involving four lakes (Mergili et al., 2018a), and the 1962 and 1970 Huascarán land-  
95 slides (Mergili et al., 2018b), both in the Cordillera Blanca. These studies identified the capability of that  
96 tool to appropriately simulate the transformations at the boundary of individual processes, where one  
97 process transforms to the next, as one of the major challenges. Open issues include the proper under-  
98 standing of wave generation as a response to landslides impacting high-mountain lakes and, as a conse-  
99 quence, the quantification of essential parameters such as the volume of overtopping water and the dis-  
100 charge (Westoby et al., 2014). Further, uncertainties in the model parameters and the initial conditions  
101 accumulate at process boundaries (Schaub et al. 2016), and threshold effects are expected to result in  
102 strongly non-linear responses of the model error (Mergili et al., 2018a, b). In high-energy mass flows,  
103 the physical characteristics of the processes involved are not always understood at the required level of  
104 detail (Mergili et al., 2018b).

105 On the one hand, flow models and simulation tools can help us to better understand some of the key  
106 mechanisms of high-mountain process chains. On the other hand, well documented case studies are  
107 important to gain a better understanding on which questions can be tackled with simulation tools, and  
108 which questions cannot be answered without further research. In the present work, we explore this field  
109 of uncertainty by applying the r.avaflow computational tool to the 1941 Lake Palcacocha GLOF process  
110 chain. Thereby, based on the simulation of different scenarios, we investigate on the following research  
111 questions:

112 1. What is the most likely release mechanism of initiating the process chain of the 1941 GLOF of  
113 Lake Palcacocha?

114        2. Are we able to back-calculate this process chain in an empirically adequate way with physically  
115        plausible model parameters? Mergili et al. (2018b) reported a trade-off between these two crite-  
116        ria for the simulation of the 1970 Huascarán landslide.

117        3. What are the major challenges in achieving successful (empirically adequate and physically plau-  
118        sible) simulations?

119        4. What can we learn with regard to forward calculations of possible future events?

120        In Sect. 2 we depict the local conditions and the documentation of the event. After having introduced  
121        the computational framework `r.avaflow` (Sect. 3), we describe in detail the simulation input (Sect. 4) and  
122        our findings (Sect. 5). We discuss the results (Sect. 6) and finally summarize the key points of the re-  
123        search (Sect. 7).

## 124        2 Lake Palcacocha

### 125        2.1 Quilcay catchment and Cojup Valley

126        Lake Palcacocha is part of a proglacial system in the headwaters of the Cojup Valley in the Cordillera  
127        Blanca, Perú (Fig. 1). This system was – and is still – shaped by the glaciers originating from the south-  
128        western slopes of Nevado Palcaraju (6,264 m a.s.l.) and Nevado Pucaranra (6,156 m a.s.l.). A prominent  
129        horseshoe-shaped ridge of lateral and terminal moraines marks the extent of the glacier during the first  
130        peak of the Little Ice Age, dated using lichenometry to the 17<sup>th</sup> Century (Emmer, 2017). With glacier  
131        retreat, the depression behind the moraine ridge was filled with a lake, named Lake Palcacocha. A pho-  
132        tograph taken by Hans Kinzl in 1939 (Kinzl and Schneider, 1950) indicates a lake level of 4,610 m a.s.l.,  
133        allowing surficial outflow (Fig. 2a). Using this photograph, Vilímek et al. (2005) estimated a lake volume  
134        between 9 and 11 million m<sup>3</sup> at that time, whereas an unpublished estimate of the Autoridad Nacional  
135        del Agua (ANA) arrived at approx. 13.1 million m<sup>3</sup>. It is assumed that the situation was essentially the  
136        same at the time of the 1941 GLOF (Sect. 2.2).

137        The Cojup Valley is part of the Quilcay catchment, draining towards southwest to the city of Huaráz,  
138        capital of the department of Ancash located at 3,090 m a.s.l. at the outlet to the Río Santa Valley  
139        (Callejon de Huaylas). The distance between Lake Palcacocha and Huaráz is approx. 23 km, whereas the  
140        vertical drop is approx. 1,500 m. The Cojup Valley forms a glacially shaped high-mountain valley in its  
141        upper part whilst cutting through the promontory of the Cordillera Blanca in its lower part. 8 km down-  
142        stream from Lake Palcacocha (15 km upstream of Huaráz), the landslide-dammed Lake Jircacocha  
143        (4.8 million m<sup>3</sup>; Vilímek et al., 2005) existed until 1941 (Andres et al., 2018). The remnants of this lake  
144        are still clearly visible in the landscape in 2017, mainly through the change in vegetation and the pres-  
145        ence of fine lake sediments (Fig. 2b). Table 1 summarizes the major characteristics of Lake Palcacocha  
146        and Lake Jircacocha before the 1941 GLOF.

### 147        2.2 1941 multi-lake outburst flood from Lake Palcacocha

148        On 13 December 1941 part of the city of Huaráz was destroyed by a catastrophic GLOF-induced debris  
149        and mud flow, with thousands of fatalities. Portocarrero (1984) gives a number of 4000 deaths, Wegner

150 (2014) a number of 1800; but this type of information has to be interpreted with care (Evans et al., 2009).  
151 The disaster was the result of a multi-lake outburst flood in the upper part of the Cojup Valley. Sudden  
152 breach of the dam and the drainage of Lake Palcacocha (Figs. 2c and e) led to a mass flow proceeding  
153 down the valley. Part of the eroded dam material, mostly coarse material, blocks and boulders, was de-  
154 posited directly downstream from the moraine dam, forming an outwash fan typical for moraine dam  
155 failures (Fig. 2c), whereas additional solid material forming the catastrophic mass flow was most likely  
156 eroded further along the flow path (both lateral and basal erosion were observed; Wegner, 2014). The  
157 impact of the flow on Lake Jircacocha led to overtopping and erosion of the landslide dam down to its  
158 base, leading to the complete and permanent disappearance of this lake. The associated uptake of the  
159 additional water and debris increased the energy of the flow, and massive erosion occurred in the steep-  
160 er downstream part of the valley, near the city of Huaráz. Reports by the local communities indicate that  
161 the valley was deepened substantially, so that the traffic between villages was interrupted. According to  
162 Somos-Valenzuela et al. (2016), the valley bottom was lowered by as much as 50 m in some parts.

163 The impact area of the 1941 multi-GLOF and the condition of Lake Palcacocha after the event are well  
164 documented through aerial imagery acquired in 1948 (Fig. 3). The image of Hans Kinzl acquired in 1939  
165 (Fig. 2a) is the only record of the status before the event. Additional information is available through  
166 eyewitness reports (Wegner, 2014). However, as Lake Palcacocha is located in a remote, uninhabited  
167 area, no direct estimates of travel times or associated flow velocities are available. Also the trigger of the  
168 sudden drainage of Lake Palcacocha remains unclear. Two mechanisms appear most likely: (i) retrogres-  
169 sive erosion, possibly triggered by an impact wave related to calving or an ice avalanche, resulting in  
170 overtopping of the dam (however, Vilímek et al., 2005 state that there are no indicators for such an im-  
171 pact); or (ii) internal erosion of the dam through piping, leading to the failure.

## 172 2.3 Lake evolution since 1941

173 As shown on the aerial images from 1948, Lake Palcacocha was drastically reduced to a small remnant  
174 proglacial pond, impounded by a basal moraine ridge within the former lake area, at a water level of  
175 4563 m a.s.l., 47 m lower than before the 1941 event (Fig. 3a). However, glacial retreat during the fol-  
176 lowing decades led to an increase of the lake area and volume (Vilímek et al., 2005). After reinforcement  
177 of the dam and the construction of an artificial drainage in the early 1970s, a lake volume of 514,800 m<sup>3</sup>  
178 was derived from bathymetric measurements (Ojeda, 1974). In 1974, two artificial dams and a perma-  
179 nent drainage channel were installed, stabilizing the lake level with a freeboard of 7 m to the dam crest  
180 (Portocarrero, 2014). By 2003, the volume had increased to 3.69 million m<sup>3</sup> (Zapata et al., 2003). In the  
181 same year, a landslide from the left lateral moraine caused a minor flood wave in the Cojup Valley  
182 (Fig. 2d). In 2016, the lake volume had increased to 17.40 million m<sup>3</sup> due to continued deglaciation  
183 (ANA, 2016). The potential of further growth is limited since, as of 2017, Lake Palcacocha is only con-  
184 nected to a small regenerating glacier. Further, the lake level is lowered artificially, using a set of siphons  
185 (it decreased by 3 m between December 2016 and July 2017). Table 1 summarizes the major characteris-  
186 tics of Lake Palcacocha in 2016. The overall situation in July 2017 is illustrated in Fig. 2c.

187 **2.4 Previous simulations of possible future GLOF process chains**

188 Due to its history, recent growth, and catchment characteristics, Lake Palcacocha is considered hazard-  
189 ous for the downstream communities, including the city of Huaráz (Fig. 2e). Whilst Vilímek et al (2005)  
190 point out that the lake volume would not allow an event comparable to 1941, by 2016 the lake volume  
191 had become much larger than the volume before 1941 (ANA, 2016). Even though the lower potential of  
192 dam erosion (Somos-Valenzuela et al., 2016) and the non-existence of Lake Jircacocha make a 1941-  
193 magnitude event appear unlikely, the steep glacierized mountain walls in the back of the lake may pro-  
194 duce ice or rock-ice avalanches leading to impact waves, dam overtopping, erosion, and subsequent mass  
195 flows. Investigations by Klimeš et al. (2016) of the steep lateral moraines surrounding the lake indicate  
196 that failures and slides from moraines are possible at several sites, but do not have the potential to create  
197 a major overtopping wave, partly due to the elongated shape of the lake. Rivas et al. (2015) elaborated on  
198 the possible effects of moraine-failure induced impact waves. Recently, Somos-Valenzuela et al. (2016)  
199 have used a combination of simulation approaches to assess the possible impact of process chains trig-  
200 gered by ice avalanching into Lake Palcacocha on Huaráz. They considered three scenarios of ice ava-  
201 lanches detaching from the slope of Palcaraju (0.5, 1.0, and 3.0 million m<sup>3</sup>) in order to create flood inten-  
202 sity maps and to indicate travel times of the mass flow to various points of interest. For the large scenar-  
203 io, the mass flow would reach the uppermost part of the city of Huaráz after approx. 1 h 20 min, for the  
204 other scenarios this time would increase to 2 h 50 min (medium scenario) and 8 h 40 min (small scenar-  
205 io). Particularly for the large scenario, a high level of hazard is identified for a considerable zone near  
206 the Quilcay River, whereas zones of medium or low hazard become more abundant with the medium  
207 and small scenarios, or with the assumption of a lowered lake level (Somos-Valenzuela et al., 2016). In  
208 addition, Chisolm and McKinney (2018) analyzed the dynamics impulse waves generated by avalanches  
209 using FLOW-3D. A similar modelling approach was applied by Frey et al. (2018) to derive a map of  
210 GLOF hazard for the Quilcay catchment. For Lake Palcacocha the same ice avalanche scenarios as ap-  
211 plied by Somos-Valenzuela et al. (2016) were employed, with correspondingly comparable results in the  
212 Cojup Valley and for the city of Huaráz.

213 **3 The r.avafow computational tool**

214 r.avafow is an open source tool for simulating the dynamics of complex mass flows in mountain areas. It  
215 employs a two-phase model including solid particles and viscous fluid, making a difference to most other  
216 mass flow simulation tools which build on one-phase mixture models. r.avafow considers the interac-  
217 tions between the phases as well as erosion and entrainment of material from the basal surface. Conse-  
218 quently, it is well-suited for the simulation of complex, cascading flow-type landslide processes. The  
219 r.avafow framework is introduced in detail by Mergili et al. (2017), only those aspects relevant for the  
220 present work are explained here.

221 The Pudasaini (2012) two-phase flow model is used for propagating mass flows from at least one defined  
222 release area through a Digital Terrain Model (DTM). Flow dynamics is computed through depth-  
223 averaged equations describing the conservation of mass and momentum for both solid and fluid. The  
224 solid stress is computed on the basis of the Mohr-Coulomb plasticity, whereas the fluid is treated with a  
225 solid-volume-fraction-gradient-enhanced non-Newtonian viscous stress. Virtual mass due to the relative

226 motion and acceleration, and generalized viscous drag, account for the strong transfer of momentum  
227 between the phases. Also buoyancy is considered. The momentum transfer results in simultaneous de-  
228 formation, separation, and mixing of the phases (Mergili et al., 2018a). Pudasaini (2012) gives a full de-  
229 description of the set of equations.

230 Certain enhancements are included, compared to the original model: for example, drag and virtual mass  
231 are computed according to extended analytical functions constructed by Pudasaini (2019a, b). Additional  
232 (complementary) functionalities include surface control, diffusion control, and basal entrainment  
233 (Mergili et al., 2017, 2018a, 2019). A conceptual model is used for entrainment: thereby, the empirically  
234 derived entrainment coefficient  $C_E$  is multiplied with the flow kinetic energy:

$$235 \quad q_{E,s} = C_E |T_s + T_f| \alpha_{s,E}, \quad q_{E,f} = C_E |T_s + T_f| (1 - \alpha_{s,E}). \quad (1)$$

236  $q_{E,s}$  and  $q_{E,f}$  ( $\text{m s}^{-1}$ ) are the solid and fluid entrainment rates,  $T_s$  and  $T_f$  (J) are the solid and fluid kinetic  
237 energies, and  $\alpha_{s,E}$  is the solid fraction of the entrainable material (Mergili et al., 2019). Flow heights and  
238 momenta as well as the change of elevation of the basal surface are updated at each time step  
239 (Mergili et al., 2017).

240 Any desired combination of solid and fluid release and entrainable heights can be defined. The main  
241 results are raster maps of the evolution of solid and fluid flow heights, velocities, and entrained heights  
242 in time. Pressures and kinetic energies are derived from the flow heights and velocities. Output hydro-  
243 graphs can be generated as an additional option (Mergili et al., 2018a). Spatial discretization works on  
244 the basis of GIS raster cells: the flow propagates between neighbouring cells during each time step. The  
245 Total Variation Diminishing Non-Oscillatory Central Differencing (TVD-NOC) Scheme (Nessyahu and  
246 Tadmor, 1990; Tai et al., 2002; Wang et al., 2004) is employed for solving the model equations. This ap-  
247 proach builds on a staggered grid, in which the system is shifted half the cell size during each step in  
248 time (Mergili et al., 2018b).

249 r.avaflow operates as a raster module of the open source software GRASS GIS 7 (GRASS Development  
250 Team, 2019), employing the programming languages Python and C as well as the R software (R Core  
251 Team, 2019). More details about r.avaflow are provided by Mergili et al. (2017).

## 252 4 Simulation input

253 The simulations build on the topography, represented by a DTM, and on particular sets of initial condi-  
254 tions and model parameters. For the DTM, we use a 5 m resolution Digital Elevation Model provided by  
255 the Peruvian Ministry of Environment, MINAM (Horizons, 2013). It was deduced from recent stereo  
256 aerial photographs and airborne LiDAR. The DEM is processed in order to derive a DTM representing  
257 the situation before the 1941 event. Thereby, we neglect the possible error introduced by the effects of  
258 vegetation or buildings, and focus on the effects of the lakes and of erosion (Fig. 4):

259 1. For the area of Lake Palcacocha the elevation of the lake surface is replaced by a DTM of the  
260 lake bathymetry derived from ANA (2016). Possible sedimentation since that time is neglected.  
261 The photograph of Hans Kinzl from 1939 (Fig. 2a) is used to reconstruct the moraine dam before  
262 the breach, and the glacier at the same time. As an exact positioning of the glacier terminus is  
263 not possible purely based on the photo, the position is optimized towards a lake volume of ap-

264 prox. 13 million m<sup>3</sup>, following the estimate of ANA. It is further assumed that there was surficial  
265 drainage of Lake Palcacocha as suggested by Fig. 2a, i.e. the lowest part of the moraine crest is set  
266 equal to the former lake level of 4,610 m a.s.l (Fig. 4b).

267 2. Also for Lake Jircacocha, surficial overflow is assumed (a situation that is observed for most of  
268 the recent landslide-dammed lakes in the Cordillera Blanca). On this basis the landslide dam be-  
269 fore its breach is reconstructed, guided by topographic and geometric considerations. The lowest  
270 point of the dam crest is set to 4,130 m a.s.l. (Fig. 4c).  
271 3. Erosional features along the flow channel are assumed to largely relate to the 1941 event. These  
272 features are filled accordingly (see Table 2 for the filled volumes). In particular, the flow channel  
273 in the lower part of the valley, reportedly deepened by up to 50 m in the 1941 event  
274 (Vilímek et al., 2005), was filled in order to represent the situation before the event in a plausible  
275 way (Fig. 4d).

276 All lakes are considered as fluid release volumes in r.avaflow. The initial level of Lake Palcacocha in  
277 1941 is set to 4,610 m a.s.l., whereas the level of Lake Jircacocha is set to 4,129 m a.s.l. The frontal part of  
278 the moraine dam impounding Lake Palcacocha and the landslide dam impounding Lake Jircacocha are  
279 considered as entrainable volumes. Further, those areas filled up along the flow path (Fig. 4d) are con-  
280 sidered entrainable, mainly following Vilímek et al. (2005). However, as it is assumed that part of the  
281 material was removed through secondary processes or afterwards, only 75% of the added material are  
282 allowed to be entrained. All entrained material is considered 80% solid and 20% fluid per volume.

283 The reconstructed lake, breach, and entrainable volumes are shown in Tables 1 and 2. The glacier termi-  
284 nus in 1941 was located in an area where the lake depth increases by several tens of metres, so that small  
285 misestimates in the position of the glacier tongue may result in large misestimates of the volume, so that  
286 some uncertainty has to be accepted.

287 As the trigger of the sudden drainage of Lake Palcacocha is not clear, we consider four scenarios, based  
288 on the situation before the event as shown in the photo taken by Hans Kinzl, experiences from other  
289 documented GLOF events in the Cordillera Blanca (Schneider et al., 2014; Mergili et al., 2018a), consid-  
290 erations by Vilímek et al. (2005), Portocarrero (2014), and Somos-Valenzuela et al. (2016), as well as  
291 geotechnical considerations:

292 A Retrogressive erosion, possibly induced by minor or moderate overtopping. This scenario is re-  
293 lated to a possible minor impact wave, caused for example by calving of ice from the glacier  
294 front, an increased lake level due to meteorological reasons, or a combination of these factors.  
295 In the simulation, the process chain is started by cutting an initial breach into the dam in order  
296 to initiate overtopping and erosion. The fluid phase is considered as pure water.

297 AX Similar to Scenario A, but with the second phase considered a mixture of fine mud and water.  
298 For this purpose, density is increased to 1,100 instead of 1,000 kg m<sup>-3</sup>, and a yield strength of  
299 5 Pa is introduced (Domnik et al., 2013; Pudasaini and Mergili, 2019; Table 3). For simplicity,  
300 we still refer to this mixture as a fluid. Such changed phase characteristics may be related to the  
301 input of fine sediment into the lake water (e.g. caused by a landslide from the lateral moraine  
302 as triggering event), but are mainly considered here in order to highlight the effects of uncer-  
303 tainties in the definition and parameterization of the two-phase mixture flow.

304 B Retrogressive erosion, induced by violent overtopping. This scenario is related to a large impact  
305 wave caused by a major rock/ice avalanche or ice avalanche rushing into the lake. In the simu-  
306 lation, the process chain is initiated through a hypothetic landslide of 3 million m<sup>3</sup> of 75% solid  
307 and 25% fluid material, following the large scenario of Somos-Valenzuela et al. (2016) in terms  
308 of volume and release area. In order to be consistent with Scenario A, fluid is considered as  
309 pure water.

310 C Internal erosion-induced failure of the moraine dam. Here, the process chain is induced by the  
311 collapse of the entire reconstructed breach volume (Fig. 4b). In the simulation, this is done by  
312 considering this part of the moraine not as entrainable volume, but as release volume (80% sol-  
313 id, 20% fluid, whereby fluid is again considered as pure water).

314 Failure of the dam of Lake Jircacocha is assumed having occurred through overtopping and retrogressive  
315 erosion, induced by the increased lake level and a minor impact wave from the flood upstream. No fur-  
316 ther assumptions of the initial conditions are required in this case.

317 The model parameter values are selected in accordance with experiences gained from previous simula-  
318 tions with r.avaflow for other study areas, and are summarized in Table 3. Three parameters mainly  
319 characterizing the flow friction (basal friction of solid  $\delta$ , ambient drag coefficient  $C_{AD}$ , and fluid friction  
320 coefficient  $C_{FF}$ ) and the entrainment coefficient  $C_E$  are optimized in a spatially differentiated way to  
321 maximize the empirical adequacy of the simulations in terms of estimates of impact areas, erosion  
322 depths, and flow and breach volumes. As no travel times or velocities are documented for the 1941  
323 event, we use the values given by Somos-Valenzuela et al. (2016) as a rough reference. Varying those  
324 four parameters while keeping the others constant helps us to capture variability while minimizing the  
325 degrees of freedom, remaining aware of possible equifinality issues (Beven, 1996; Beven and Freer,  
326 2001).

327 A particularly uncertain parameter is the empirical entrainment coefficient  $C_E$  (Eq. 1). In order to opti-  
328 mize  $C_E$ , we consider (i) successful prediction of the reconstructed breach volumes; and (ii) correspond-  
329 ence of peak discharge with published empirical equations on the relation between peak discharge, and  
330 lake volume and dam height (Walder and O'Connor, 1997). Table 4 summarizes these equations for mo-  
331 raine dams (applied to Lake Palcacocha) and landslide dams (applied to Lake Jircacocha), and the values  
332 obtained for the regression and the envelope, using the volumes of both lakes. We note that Table 4 re-  
333 veals very large differences – roughly one order of magnitude – between regression and envelope. In  
334 case of the breach of the moraine dam of Lake Palcacocha, we consider an extreme event due to the  
335 steep, poorly consolidated, and maybe soaked moraine, with a peak discharge close to the envelope (ap-  
336 prox.. 15,000 m<sup>3</sup> s<sup>-1</sup>). For Lake Jircacocha, in contrast, the envelope values of peak discharge do not ap-  
337 pear realistic. However, due to the high rate of water inflow from above, a value well above the regres-  
338 sion line still appears plausible, even though the usefulness of the empirical laws for this type of lake  
339 drainage can be questioned. The value of  $C_E$  optimized for the dam of Lake Jircacocha is also used for  
340 entrainment along the flow path.

341 All of the computational experiments are run with 10 m spatial resolution. Only flow heights  $\geq 25$  cm are  
342 considered for visualization and evaluation. We now describe one representative simulation result for

343 each of the considered scenarios, thereby spanning the most plausible and empirically adequate field of  
344 simulations.

## 345 5 ravaflow simulation results

### 346 5.1 Scenario A – Event induced by overtopping; fluid without yield strength

347 Outflow from Lake Palcacocha starts immediately, leading to (1) lowering of the lake level and (2) retro-  
348 gressive erosion of the moraine dam. The bell-shaped fluid discharge curve at the hydrograph profile O1  
349 (Fig. 4) reaches its peak of  $18,700 \text{ m}^3 \text{ s}^{-1}$  after approx. 780 s, and then decreases to a small residual  
350 (Fig. 5a). Channel incision happens quickly – 53 m of lowering of the terrain at the reference point R1  
351 occurs in the first less than 1200 s, whereas the lowering at the end of the simulation is 60 m (Fig. 6a).  
352 This number represents an underestimation, compared to the reference value of 76 m (Table 2). The lake  
353 level decreases by 42 m, whereby 36.5 m of the decrease occur within the first 1200 s. The slight under-  
354 estimation, compared to the reference value of 47 m of lake level decrease, is most likely a consequence  
355 of uncertainties in the topographic reconstruction. A total amount of 1.5 million  $\text{m}^3$  is eroded from the  
356 moraine dam of Lake Palcacocha, corresponding to an underestimation of 22%, compared to the recon-  
357 structed breach volume. Underestimations mainly occur at both sides of the lateral parts of the eroded  
358 channel near the moraine crest – an area where additional post-event erosion can be expected, so that  
359 the patterns and degree of underestimation appear plausible (Fig. 7a). In contrast, some overestimation  
360 of erosion occurs in the inner part of the dam. For numerical reasons, some minor erosion is also simu-  
361 lated away from the eroded channel. The iterative optimization procedure results in an entrainment  
362 coefficient  $C_E = 10^{-6.75}$ .

363 The deposit of much of the solid material eroded from the moraine dam directly downstream from Lake  
364 Palcacocha, as observed in the field (Fig. 2c), is reasonably well reproduced by this simulation, so that  
365 the flow proceeding down-valley is dominated by the fluid phase (Fig. 8). It reaches Lake Jircacocha  
366 after  $t = 840 \text{ s}$  (Fig. 5b). As the inflow occurs smoothly, there is no impact wave in the strict sense, but it  
367 is rather the steadily rising water level (see Fig. 6b for the evolution of the water level at the reference  
368 point R2) inducing overtopping and erosion of the dam. This only starts gradually after some lag time, at  
369 approx.  $t = 1,200 \text{ s}$ . The discharge curve at the profile O2 (Fig. 4) reaches its pronounced peak of  
370  $750 \text{ m}^3 \text{ s}^{-1}$  solid and  $14,700 \text{ m}^3 \text{ s}^{-1}$  fluid material at  $t = 2,340 \text{ s}$ , and then tails off slowly.

371 In the case of Lake Jircacocha, the simulated breach is clearly shifted south, compared to the observed  
372 breach. With the optimized value of the entrainment coefficient  $C_E = 10^{-7.15}$ , the breach volume is under-  
373 estimated by 24%, compared to the reconstruction (Fig. 7b). Also here, this intentionally introduced  
374 discrepancy accounts for some post-event erosion. However, we note that volumes are uncertain as the  
375 reconstruction of the dam of Lake Jircacocha – in contrast to Lake Palcacocha – is a rough estimation  
376 due to lacking reference data.

377 Due to erosion of the dam of Lake Jircacocha, and also erosion of the valley bottom and slopes, the solid  
378 fraction of the flow increases considerably downstream. Much of the solid material, however, is deposi-  
379 ed in the lateral parts of the flow channel, so that the flow arriving at Huaráz is fluid-dominated again  
380 (Fig. 8). The front enters the alluvial fan of Huaráz at  $t = 2,760 \text{ s}$ , whereas the broad peak of  $10,500 \text{ m}^3 \text{ s}^{-1}$

381 of fluid and  $2,000 \text{ m}^3 \text{ s}^{-1}$  of solid material (solid fraction of 16%) is reached in the period between 3,600  
382 and 3,780 s (Fig. 4; Fig. 5c). Discharge decreases steadily afterwards. A total of 2.5 million  $\text{m}^3$  of solid and  
383 14.0 million  $\text{m}^3$  of fluid material pass the hydrograph profile O3 until  $t = 5,400$  s. Referring only to the  
384 solid, this is less material than reported by Kaser and Georges (2003). However, (i) there is still some  
385 material coming after, and (ii) pore volume has to be added to the solid volume, so that the order of  
386 magnitude of material delivered to Huaráz corresponds to the documentation in a better way. Still, the  
387 solid ratio of the hydrograph might represent an underestimation.

388 As prescribed by the parameter optimization, the volumes entrained along the channel are in the same  
389 order of magnitude, but lower than the reconstructed volumes summarized in Table 2: 0.7 million  $\text{m}^3$  of  
390 material are entrained upstream and 1.5 million  $\text{m}^3$  downstream of Lake Jircacocha, and 5.3 million  $\text{m}^3$   
391 in the promontory. Fig. 9a summarizes the travel times and the flow velocities of the entire process  
392 chain. Frontal velocities mostly vary between  $5 \text{ m s}^{-1}$  and  $20 \text{ m s}^{-1}$ , with the higher values in the steeper  
393 part below Lake Jircacocha. The low and undefined velocities directly downstream of Lake Jircacocha  
394 reflect the time lag of substantial overtopping. The key numbers in terms of times, discharges, and vol-  
395 umes are summarized in Table 5.

## 396 5.2 Scenario AX – Event induced by overtopping; fluid with yield strength

397 Adding a yield strength of  $\tau_y = 5 \text{ Pa}$  to the characteristics of the fluid substantially changes the temporal  
398 rather than the spatial evolution of the process cascade. As the fluid now behaves as fine mud instead of  
399 water and is more resistant to motion, velocities are lower, travel times are much longer, and the en-  
400 trained volumes are smaller than in the Scenario A (Fig. 9b; Table 5). The peak discharge at the outlet of  
401 Lake Palcacocha is reached at  $t = 1,800$  s. Fluid peak discharge of  $8,200 \text{ m}^3 \text{ s}^{-1}$  is less than half the value  
402 yielded in Scenario A (Fig. 5d). The volume of material eroded from the dam is only slightly smaller  
403 than in Scenario A (1.4 versus 1.5 million  $\text{m}^3$ ). The numerically induced false positives with regard to  
404 erosion observed in Scenario A are not observed in Scenario AX, as the resistance to oscillations in the  
405 lake is higher with the added yield strength (Fig. 7c). Still, the major patterns of erosion and entrain-  
406 ment are the same. Interestingly, erosion is deeper in Scenario AX, reaching 76 m at the end of the simu-  
407 lation (Fig. 6c) and therefore the base of the entrainable material (Table 2). This is most likely a conse-  
408 quence of the spatially more concentrated flow and therefore higher erosion rates along the centre of  
409 the breach channel, with less lateral spreading than in Scenario A.

410 Consequently, also Lake Jircacocha is reached later than in Scenario A (Fig. 6d), and the peak discharge  
411 at its outlet is delayed ( $t = 4,320$  s) and lower ( $7,600 \text{ m}^3 \text{ s}^{-1}$  of fluid and  $320 \text{ m}^3 \text{ s}^{-1}$  of solid material)  
412 (Fig. 5e). 2.0 million  $\text{m}^3$  of material are entrained from the dam of Lake Jircacocha, with similar spatial  
413 patterns as in Scenario A (Fig. 7d). Huaráz is reached after  $t = 4,200$  s, and the peak discharge of  
414  $5,000 \text{ m}^3 \text{ s}^{-1}$  of fluid and  $640 \text{ m}^3 \text{ s}^{-1}$  of solid material at O3 occurs after  $t = 6,480$  s (Fig. 5f). This corre-  
415 sponds to a solid ratio of 11%. Interpretation of the solid ratio requires care here as the fluid is defined as  
416 fine mud, so that the water content is much lower than the remaining 89%. The volumes entrained  
417 along the flow channel are similar in magnitude to those obtained in the simulation of Scenario A (Ta-  
418 ble 5).

419 **5.3 Scenario B – Event induced by impact wave**

420 Scenario B is based on the assumption of an impact wave from a 3 million m<sup>3</sup> landslide. However, due to  
421 the relatively gently-sloped glacier tongue heading into Lake Palcacocha at the time of the 1941 event  
422 (Figs. 2a and 4b), only a small fraction of the initial landslide volume reaches the lake, and impact ve-  
423 locities and energies are reduced, compared to a direct impact from the steep slope. Approx. 1 million m<sup>3</sup>  
424 of the landslide have entered the lake until  $t = 120$  s, an amount which only slightly increases thereafter.  
425 Most of the landslide deposits on the glacier surface. Caused by the impact wave, discharge at the outlet  
426 of Lake Palcacocha (O1) sets on at  $t = 95$  s and, due to overtopping of the impact wave, immediately  
427 reaches a relatively moderate first peak of 7,000 m<sup>3</sup> s<sup>-1</sup> of fluid discharge. The main peak of 16,900 m<sup>3</sup> s<sup>-1</sup>  
428 of fluid and 2,000 m<sup>3</sup> s<sup>-1</sup> of solid discharge occurs at  $t = 1,200$  s due to the erosion of the breach channel.  
429 Afterwards, discharge decreases relatively quickly to a low base level (Fig. 10a). The optimized value of  
430  $C_E = 10^{-6.75}$  is used also for this scenario. The depth of erosion along the main path of the breach channel  
431 is clearly less than in the Scenario A (Fig. 6e). However, Table 5 shows a higher volume of eroded dam  
432 material than the other scenarios. These two contradicting patterns are explained by Fig. 11a: the over-  
433 topping due to the impact wave does not only initiate erosion of the main breach, but also of a secondary  
434 breach farther north. Consequently, discharge is split among the two breaches and therefore less con-  
435 centrated, explaining the lower erosion at the main channel despite a larger total amount of eroded ma-  
436 terial. The secondary drainage channel can also be deduced from observations (Fig. 3a), but has probably  
437 played a less important role than suggested by this simulation.

438 The downstream results of Scenario B largely correspond to the results of the Scenario A, with some  
439 delay partly related to the time from the initial landslide to the overtopping of the impact wave. Dis-  
440 charge at the outlet of Lake Jircacocha peaks at  $t = 2,700$  s (Fig. 10b), and the alluvial fan of Huaráz is  
441 reached after 3,060 s (Fig. 10c). The peak discharges at O2 and O3 are similar to those obtained in the  
442 Scenario A. The erosion patterns at the dam of Lake Jircacocha (again,  $C_E = 10^{-7.15}$ ) very much resemble  
443 those yielded with the scenarios A and AX (Fig. 11b), and so does the volume of entrained dam material  
444 (2.2 million m<sup>3</sup>). The same is true for the 2.5 million m<sup>3</sup> of solid and 13.9 million m<sup>3</sup> of fluid material  
445 entering the area of Huaráz until  $t = 5,400$  s, according to this simulation.

446 Also in this scenario, the volumes entrained along the flow channel are very similar to those obtained in  
447 the simulation of Scenario A. The travel times and frontal velocities – resembling the patterns obtained  
448 in Scenario A, with the exception of the delay – are shown in Fig. 12a, whereas Table 5 summarizes the  
449 key numbers in terms of times, volumes, and discharges.

450 **5.4 Scenario C – Event induced by dam collapse**

451 In Scenario C, we assume that the breached part of the moraine dam collapses, the collapsed mass mixes  
452 with the water from the suddenly draining lake, and flows downstream. The more sudden and powerful  
453 release, compared to the two other scenarios, leads to higher frontal velocities and shorter travel times  
454 (Fig. 12b; Table 5).

455 In contrast to the other scenarios, impact downstream starts earlier, as more material is released at once,  
456 instead of steadily increasing retrogressive erosion and lowering of the lake level. The fluid discharge at  
457 O1 peaks at almost 40,000 m<sup>3</sup> s<sup>-1</sup> (Fig. 10d) rapidly after release. Consequently, Lake Jircacocha is

458 reached already after 720 s, and the impact wave in the lake evolves more quickly than in all the other  
459 scenarios considered (Fig. 6f). The lake drains with a peak discharge of  $15,400 \text{ m}^3 \text{ s}^{-1}$  of fluid and  
460  $830 \text{ m}^3 \text{ s}^{-1}$  of solid material after 1,680–1,740 s (Fig. 10e). In contrast to the more rapid evolution of the  
461 process chain, discharge magnitudes are largely comparable to those obtained with the other scenarios.  
462 The same is true for the hydrograph profile O3: the flow reaches the alluvial fan of Huaráz after  
463  $t = 2,160$  s, with a peak discharge slightly exceeding  $10,000 \text{ m}^3 \text{ s}^{-1}$  of fluid and  $2,000 \text{ m}^3 \text{ s}^{-1}$  of solid mate-  
464 rial between  $t = 2,940$  s and  $3,240$  s. 2.7 million  $\text{m}^3$  of solid and 14.6 million  $\text{m}^3$  of fluid material enter  
465 the area of Huaráz until  $t = 5,400$  s, which is slightly more than in the other scenarios, indicating the  
466 more powerful dynamics of the flow (Table 5). The fraction of solid material arriving at Huaráz remains  
467 low, with 16% solid at peak discharge and 15% in total. Again, the volumes entrained along the flow  
468 channel are very similar to those obtained with the simulations of the other scenarios (Table 5).

## 469 6 Discussion

### 470 6.1 Possible trigger of the GLOF process chain

471 In contrast to other GLOF process chains in the Cordillera Blanca, such as the 2010 event at Laguna 513  
472 (Schneider et al., 2014), which was clearly triggered by an ice-rock avalanche into the lake, there is dis-  
473 agreement upon the trigger of the 1941 multi-lake outburst flood in the Quilcay catchment. Whereas,  
474 according to contemporary reports, there is no evidence of a landslide (for example, ice avalanche) im-  
475 pact onto the lake (Vilímek et al., 2005; Wegner, 2014), and dam rupture would have been triggered by  
476 internal erosion, some authors postulate an at least small impact starting the process chain (Portocarrero,  
477 2014; Somos-Valenzuela et al., 2016).

478 Each of the three assumed initiation mechanisms of the 1941 event, represented by the Scenarios A/AX,  
479 B, and C, yields results which are plausible in principle. We consider a combination of all three mecha-  
480 nisms a likely cause of this extreme process chain. Overtopping of the moraine dam, possibly related to a  
481 minor impact wave, leads to the best correspondence of the model results with the observation, docu-  
482 mentation, and reconstruction. Particularly the signs of minor erosion of the moraine dam north of the  
483 main breach (Fig. 3a) support this conclusion: a major impact wave, resulting in violent overtopping of  
484 the entire frontal part of the moraine dam, would supposedly also have led to more pronounced erosion  
485 in that area, as to some extent predicted by the Scenario B. There is also no evidence for strong land-  
486 slide-glacier interactions (massive entrainment of ice or even detachment of the glacier tongue) which  
487 would be likely scenarios in the case of a very large landslide. Anyway, the observations do not allow for  
488 substantial conclusions on the volume of a hypothetic triggering landslide: as suggested by Scenario B,  
489 even a large landslide from the slopes of Palcaraju or Pucaranra could have been partly alleviated on the  
490 rather gently sloped glacier tongue between the likely release area and Lake Palcacocha.

491 The minor erosional feature north of the main breach was already visible in the photo of Kinzl (Fig. 2a),  
492 possibly indicating an earlier, small GLOF. It remains unclear whether it was reactivated in 1941. Such a  
493 reactivation could only be directly explained by an impact wave, but not by retrogressive erosion only  
494 (A/AX) or internal failure of the dam (C) – so, more research is needed here. The source area of a possi-  
495 ble impacting landslide could have been the slopes of Palcaraju or Pucaranra (Fig. 1), or the calving glac-

496 ier front (Fig. 2a). Attempts to quantify the most likely release volume and material composition would  
497 be considered speculative due to the remaining difficulties in adequately simulating landslide-(glacier-  
498 )lake interactions (Westoby et al., 2014). Further research is necessary in this direction. In any case, a  
499 poor stability condition of the dam (factor of safety  $\sim 1$ ) could have facilitated the major retrogressive  
500 erosion of the main breach. A better understanding of the hydro-mechanical load applied by a possible  
501 overtopping wave and the mechanical strength of the moraine dam could help to resolve this issue.

502 The downstream patterns of the flow are largely similar for each of the scenarios A, AX, B, and C, with  
503 the exception of travel times and velocities. Interaction with Lake Jircacocha disguises much of the sig-  
504 nal of process initiation. Lag times between the impact of the flow front on Lake Jircacocha and the on-  
505 set of substantial overtopping and erosion are approx. 10 minutes in the scenarios A and B, and less than  
506 3 minutes in the Scenario C. This clearly reflects the slow and steady onset of those flows generated  
507 through retrogressive erosion. The moderate initial overtopping in Scenario B seems to alleviate before  
508 reaching Lake Jircacocha. Sudden mechanical failure of the dam (Scenario C), in contrast, leads to a  
509 more sudden evolution of the flow, with more immediate downstream consequences.

## 510 6.2 Parameter uncertainties

511 We have tried to back-calculate the 1941 event in a way reasonably corresponding to the observation,  
512 documentation and reconstruction, and building on physically plausible parameter sets. Earlier work on  
513 the Huascarán landslides of 1962 and 1970 has demonstrated that empirically adequate back-calculations  
514 are not necessarily plausible with regard to parameterization (Mergili et al., 2018b). This issue may be  
515 connected to equifinality issues (Beven, 1996; Beven and Freer, 2001), and in the case of the very ex-  
516 treme and complex Huascarán 1970 event, by the inability of the flow model and its numerical solution  
517 to adequately reproduce some of the process components (Mergili et al., 2018b). In the present work,  
518 however, reasonable levels of empirical adequacy and physical plausibility are achieved. Open questions  
519 remain with regard to the spatial differentiation of the basal friction angle required to obtain adequate  
520 results (Table 3): lower values of  $\delta$  downstream from the dam of Lake Jircacocha are necessary to ensure  
521 that a certain fraction of solid passes the hydrograph profile O3 and reaches Huaráz. Still, solid fractions  
522 at O3 appear rather low in all simulations. A better understanding of the interplay between friction,  
523 drag, virtual mass, entrainment, deposition, and phase separation could help to resolve this issue (Puda-  
524 saini and Fischer, 2016a, b; Pudasaini, 2019a, b).

525 The empirically adequate reproduction of the documented spatial patterns is only one part of the story  
526 (Mergili et al., 2018a). The dynamic flow characteristics (velocities, travel times, hydrographs) are com-  
527 monly much less well documented, particularly for events in remote areas which happened a long time  
528 ago. Therefore, direct references for evaluating the empirical adequacy of the dimension of time in the  
529 simulation results are lacking. However, travel times play a crucial role related to the planning and de-  
530 sign of (early) warning systems and risk reduction measures (Hofflinger et al., 2019). Comparison of the  
531 results of the scenarios A and AX (Fig. 9) reveals almost doubling travel times when adding a yield stress  
532 to the fluid fraction. In both scenarios, the travel times to Huaráz are within the same order of magni-  
533 tude as the travel times simulated by Somos-Valenzuela et al. (2016) and therefore considered plausible,  
534 so that it is hard to decide about the more adequate assumption. Even though the strategy of using the

535 results of earlier simulations as reference may increase the robustness of model results, it might also re-  
536 produce errors and inaccuracies of earlier simulation attempts, and thereby confirm wrong results.

537 The large amount of more or less pure lake water would point towards the Scenario A, whereas intense  
538 mixing and entrainment of fine material would favour the Scenario AX. More work is necessary in this  
539 direction, also considering possible phase transformations (Pudasaini and Krautblatter, 2014). At the  
540 same time, the optimization and evaluation of the simulated discharges remains a challenge. Here we  
541 rely on empirical relationships gained from the analysis of comparable events (Walder and O'Connor,  
542 1997).

### 543 6.3 Implications for predictive simulations

544 Considering what was said above, the findings from the back-calculation of the 1941 event can help us  
545 to better understand and constrain possible mechanisms of this extreme process chain. In principle, such  
546 an understanding can be transferred to present hazardous situations in order to inform the design of  
547 technical remediation measures. Earlier, measures were not only implemented at Lake Palcacocha (Por-  
548 tocarrero, 2014), but also at various other lakes such as Laguna 513: a tunnelling scheme implemented in  
549 the 1990s strongly reduced the impacts of the 2010 GLOF process chain (Reynolds, 1998; Reynolds et al.,  
550 1998; Schneider et al., 2014).

551 However, the findings of this study should only be applied for forward simulations in the same area or  
552 other areas with utmost care. The initial conditions and model parameters are not necessarily valid for  
553 events of different characteristics and magnitudes (Mergili et al., 2018b). In the case of Lake Palcacocha,  
554 the situation has changed substantially since 1941: the lake level is much lower and the volume larger,  
555 and the lake is directly connected to the steep glacierized slopes, so that the impact of a hypothetic land-  
556 slide could be very different now. Also, the current lake is dammed by another moraine than the pre-  
557 1941 lake, with a very different dam geometry (Somos-Valenzuela et al., 2016). In general, the mecha-  
558 nisms of the landslide impact into the lake, which were not the focus of the present study, would require  
559 more detailed investigations. Ideally, such work would be based on a three-phase model (Pudasaini and  
560 Mergili, 2019; considering ice as a separate phase), and consider knowledge and experience gained from  
561 comparable, well-documented events. A possible candidate for such an event would be the 2010 event at  
562 Laguna 513, which was back-calculated by Schneider et al. (2014). In general, it remains a challenge to  
563 reliably predict the outcomes of given future scenarios. The magnitude of the 1941 event was amplified  
564 by the interaction with Lake Jircacocha, whereas the 2012 GLOF process chain in the Santa Cruz Valley  
565 (Mergili et al., 2018a) alleviated due to the interaction with Lake Jatuncocha, comparable in size. While  
566 it seems clear that the result of such an interaction depends on event magnitude, topography, and the  
567 dam characteristics of the impacted lake, Mergili et al. (2018a, b) have demonstrated the high sensitivity  
568 of the behaviour of the simulated flow to the friction parameters, but also to the material involved (re-  
569 lease mass, entrainment). A larger number of back-calculated process chains will be necessary to derive  
570 guiding parameter sets which could facilitate predictive simulations, and so will an appropriate consider-  
571 ation of model uncertainties and possible threshold effects (Mergili et al., 2018b). Earlier studies, consid-  
572 ering the 2010 event at Laguna 513 (Schneider et al., 2014) and three future scenarios for Lake Palcaco-  
573 cha (Somos-Valenzuela et al., 2016) have followed a different strategy, using model cascades instead on

574 integrated simulations, so that a comparison with studies based on r.avaflow is only possible to a limited  
575 extent.

576 Another remaining issue is the lateral spreading of the flow on the fan of Huaráz, which is overestimated  
577 in all four simulations (Figs. 8, 9, and 12): the most likely reason for this is the insufficient representation  
578 of fine-scale structures such as buildings or walls in the DEM, which would serve as obstacles confining  
579 the flow in lateral direction.

## 580 **7 Conclusions**

581 We have performed back-calculations of the documented 1941 GLOF process chain involving Lake Pal-  
582 cacocha and Lake Jircacocha in the Quilcay catchment in the Cordillera Blanca, Perú. The key messages  
583 of this work are summarized as follows:

- 584 • Retrogressive erosion, possibly caused by a minor impact wave, appears to be the most likely re-  
585 lease mechanism of the process chain, facilitated by a geotechnically poorly stable dam with a  
586 low width-to-height ratio. This type of failure – a combination of the idealized scenarios consid-  
587 ered in this work – can be inferred from observations, and appears most plausible with regard to  
588 the simulation results. The identification of the triggering process remains difficult, also because  
589 the subsequent interaction with Lake Jircacocha disguises part of the respective signature down-  
590 stream.
- 591 • The correspondence between simulation results and observations is reasonable, and the model  
592 parameter values used are physically plausible. However, considerable uncertainties remain with  
593 regard to peaks and shapes of the discharge hydrographs, and to the quantification of flow veloc-  
594 ities and travel times. Adding a yield strength to the fluid phase (Scenario AX) completely  
595 changes the temporal, but not the spatial evolution of the flow. Still, travel times remain in the  
596 same order of magnitude as those derived by Somos-Valenzuela et al. (2016) for possible future  
597 events.
- 598 • Transfer of the findings to forward simulations in the same area or elsewhere remains a chal-  
599 lenge due to differences in the initial conditions, uncertainties of the reference data, equifinality  
600 issues, and the effects of process magnitude (Mergili et al., 2018b).

## 601 **Code availability**

602 The model codes of r.avaflow, a manual, training data, and the necessary start scripts can be obtained  
603 from Mergili and Pudasaini (2019).

## 604 **Data availability**

605 The original DEM was provided by MINAM and may not be freely distributed, but all data derived  
606 within the present work can be obtained by directly contacting the first author (mar-  
607 tin.mergili@boku.ac.at).

## 608 **Author contribution**

609 MM developed the main ideas, defined the scenarios, did most of the data processing, simulations, and  
610 analyses, wrote the major portion of the text, and prepared all the figures and tables. SP provided im-  
611 portant ideas with regard to the numerical simulations and contributed to the internal revision and op-  
612 timization of the manuscript. AE contributed with important ideas, conducted field work, acquired data,  
613 contributed to the writing of the introductory chapters, and took part in the internal revision and opti-  
614 mization of the manuscript. JTF provided important contributions to the internal revision and optimiza-  
615 tion of the work. AC provided important data and contributed to the internal revision and optimization  
616 of the manuscript. HF contributed with important ideas and field work, data acquisition, and text blocks  
617 for the introductory chapters, and took part in the internal revision and optimization of the manuscript.

## 618 **Competing interests**

619 The authors declare that they have no conflict of interest.

## 620 **Acknowledgements**

621 Part of this work was conducted within the international cooperation project “A GIS simulation model  
622 for avalanche and debris flows (avaflow)” supported by the German Research Foundation (DFG, project  
623 number PU 386/3-1) and the Austrian Science Fund (FWF, project number I 1600-N30). Shiva P. Puda-  
624 saini further acknowledges financial support from DFG through the research project “A novel and uni-  
625 fied solution to multi-phase mass flows: U\_MultiSol”. The work also follows the AKTION Austria –  
626 Czech Republic project “Currently forming glacial lakes: potentially hazardous entities in deglaciating  
627 high mountains” of Adam Emmer and Martin Mergili. Further, the support provided by the Swiss Agen-  
628 cy for Development and Cooperation (SDC) through Proyecto Glaciares+, is acknowledged. Adam Em-  
629 mer was also supported by the Ministry of Education, Youth and Sports of the Czech Republic within  
630 the National Sustainability Programme I (NPU I), grant number LO1415, and the postdoc grant of the  
631 Czech Academy of Sciences. Finally, we are grateful to Matthias Benedikt for comprehensive technical  
632 support in relation to r.avaflow.

## 633 **References**

634 ANA: *Inventario Nacional de Glaciares y Lagunas – Lagunas*, Ministerio de Agricultura y Riesgo, Autori-  
635 dad Nacional del Agua, Unidad de Glaciología y Recursos Hídricos, Huaráz, Peru, 2014.

636 ANA: *Plano batimétrico de la Laguna Palcacocha. Perfil longitudinal y transversal*, Ministerio de Agri-  
637 cultura y Riesgo, Autoridad Nacional del Agua, Unidad de Glaciología y Recursos Hídricos, Huaráz, Pe-  
638 ru, 2016.

639 Andres, C. N., Eyles, C. H., Jara, H., and Narro-Pérez, R.: *Sedimentological analysis of Paleolake Jircaco-  
640 cha, Cojup Valley, Cordillera Blanca, Peru*. *Revista de Glaciares y Ecosistemas de Montaña*, 5, 9–26,  
641 2018.

642 Beven, K.: Equifinality and Uncertainty in Geomorphological Modelling, in: The Scientific Nature of  
643 Geomorphology: Proceedings of the 27th Binghamton Symposium in Geomorphology, 27-29 September  
644 1996, John Wiley & Sons, 289–313, 1996.

645 Beven, K., and Freer, J.: Equifinality, data assimilation, and uncertainty estimation in mechanistic mod-  
646 elling of complex environmental systems using the GLUE methodology, *J. Hydrol.*, 249(1), 11–29,  
647 [https://doi.org/10.1016/S0022-1694\(01\)00421-8](https://doi.org/10.1016/S0022-1694(01)00421-8), 2001.

648 Bolch, T., Peters, J., Yegorov, A., Prafhan, B., Buchroithner, M., and Blagoveshchensky, V.: Identifica-  
649 tion of potentially dangerous glacial lakes in the northern Tien Shan, *Nat. Hazards*, 59, 1691–1714,  
650 <https://doi.org/10.1007/s11069-011-9860-2>, 2011.

651 Breien, H., De Blasio, F. V., Elverhoi, A., and Hoeg, K.: Erosion and morphology of a debris flow caused  
652 by a glacial lake outburst flood, Western Norway, *Landslides*, 5(3), 271–280,  
653 <https://doi.org/10.1007/s10346-008-0118-3>, 2008.

654 Broggi, J. A.: Informe preliminar sobre la exploracion y estudio de las condiciones de estabilidad de las  
655 lagunas de la Cordillera Blanca, ELECTROPERU S.A., Lima, Peru, 1942.

656 Carey, M.: Living and dying with glaciers: people's historical vulnerability to avalanches and outburst  
657 floods in Peru. *Glob. Planet. Change*, 47, 122–134, <https://doi.org/10.1016/j.gloplacha.2004.10.007>, 2005.

658 Carey, M., Huggel, C., Bury, J., Portocarrero, C., and Haeberli, W.: An integrated socio-environmental  
659 framework for glacier hazard management and climate change adaptation: lessons from Lake 513, Cor-  
660 dillera Blanca, Peru, *Clim. Change*, 112(3), 733–767, <https://doi.org/10.1007/s10584-011-0249-8>, 2012.

661 Carey, M., McDowell, G., Huggel, C., Jackson, M., Portocarrero, C., Reynolds, J.M., and Vicuña, L.: Inte-  
662 grated approaches to adaptation and disaster risk reduction in dynamic socio-cryospheric systems, in:  
663 Snow and Ice-related Hazards, Risks and Disasters, edited by: Haeberli, W., and Whiteman, C., 219–261,  
664 Elsevier, <https://doi.org/10.1016/B978-0-12-394849-6.00008-1>, 2014.

665 Chisolm, R. E., and McKinney, D. C.: Dynamics of avalanche-generated impulse waves: three-  
666 dimensional hydrodynamic simulations and sensitivity analysis, *Nat. Hazards Earth Syst. Sci.*, 18, 1373–  
667 1393, <https://doi.org/10.5194/nhess-18-1373-2018>, 2018.

668 Christen, M., Kowalski, J., and Bartelt, P.: RAMMS: Numerical simulation of dense snow ava-lanches in  
669 three-dimensional terrain, *Cold Reg. Sci. Technol.*, 63, 1–14,  
670 <https://doi.org/10.1016/j.coldregions.2010.04.005>, 2010.

671 Clague, J. J., and O'Connor, J. E.: Glacier-related outburst floods, in: Snow and Ice-related Hazards, Risks  
672 and Disasters, edited by: Haeberli, W., and Whiteman, C., 487–519, Elsevier,  
673 <https://doi.org/10.1016/B978-0-12-394849-6.00014-7>, 2014.

674 Concha, J. F.: Sintesis de los trabajos efectuados por la comision de las lagunas de la Cordillera Blanca,  
675 Ministerio de Fomento, Comision de Control de las Lagunas de la Cordillera Blanca (CCLCB), Lima, Pe-  
676 ru, 1952.

677 Domnik, B., Pudasaini, S. P., Katzenbach, R., and Miller, S. A.: Coupling of full two-dimensional and  
678 depth-averaged models for granular flows, *J. Non-Newtonian Fluid Mech.*, 201, 56–68,  
679 <https://doi.org/10.1016/j.jnnfm.2013.07.005>, 2013.

680 Emmer, A.: Geomorphologically effective floods from moraine-dammed lakes in the Cordillera Blanca,  
681 Peru, *Quat. Sci. Rev.*, 177, 220–234, <https://doi.org/10.1016/j.quascirev.2017.10.028>, 2017.

682 Emmer, A., and Vilímek, V.: Review Article: Lake and breach hazard assessment for moraine-dammed  
683 lakes: an example from the Cordillera Blanca (Peru), *Nat. Hazards Earth Syst. Sci.*, 13, 1551–1565,  
684 <https://doi.org/10.5194/nhess-13-1551-2013>, 2013.

685 Emmer, A., and Vilímek, V.: New method for assessing the susceptibility of glacial lakes to outburst  
686 floods in the Cordillera Blanca, Peru, *Hydrol. Earth Syst. Sci.*, 18, 3461–3479,  
687 <https://doi.org/10.5194/hess-18-3461-2014>, 2014.

688 Emmer, A., Klimeš, J., Mergili, M., Vilímek, V., and Cochachin, A.: 882 lakes of the Cordillera Blanca: an  
689 inventory, classification and assessment of susceptibility to outburst flood, *Catena*, 147, 269–279,  
690 <https://doi.org/10.1016/j.catena.2016.07.032>, 2016.

691 Emmer, A., Merkl, S., and Mergili, M.: Spatiotemporal patterns of high-mountain lakes and related haz-  
692 ards in western Austria, *Geomorphology*, 246, 602–616, <https://doi.org/10.1016/j.geomorph.2015.06.032>,  
693 2015.

694 Emmer, A., Vilímek, V., and Zapata, M. L.: Hazard mitigation of glacial lake outburst floods in the Cor-  
695 dillera Blanca (Peru): the effectiveness of remedial works, *J. Flood Risk Manag.*, 11, 489–501,  
696 <https://doi.org/10.1111/jfr3.12241>, 2018.

697 Emmer, A., Harrison, S., Mergili, M., Allen, S., Frey, H., and Huggel, C.: A 70 year record of lake evolu-  
698 tion and Glacial Lake Outburst Floods in the Peruvian Andes, *Proc. Natl. Acad. Sci. U. S. A.*, submitted  
699 manuscript, 2019.

700 Evans, S. G., Bishop, N.F., Fidel Smoll, L., Valderrama Murillo, P., Delaney, K.B., and Oliver-Smith, A.:  
701 A re-examination of the mechanism and human impact of catastrophic mass flows originating on Neva-  
702 do Huascarán, Cordillera Blanca, Peru in 1962 and 1970, *Eng. Geol.*, 108, 96–118,  
703 <https://doi.org/10.1016/j.enggeo.2009.06.020>, 2009.

704 Frey, H., Huggel, C., Chisom, R. E., Baer, P., Mc Ardell, B., Cochachin, A., and Portocarrero, C.: Multi-  
705 Source Glacial Lake Outburst Flood Hazard Assessment and Mapping for Huaráz, Cordillera Blanca, Pe-  
706 ru, *Front. Earth Sci.*, 6, 210, <https://doi.org/10.3389/feart.2018.00210>, 2018.

707 Gabl, R., Seibl, J., Gems, B., and Aufleger, M.: 3-D numerical approach to simulate the overtopping vol-  
708 ume caused by an impulse wave comparable to avalanche impact in a reservoir, *Nat. Hazards Earth Syst.*  
709 *Sci.*, 15, 2617–2630, <https://doi.org/10.5194/nhess-15-2617-2015>, 2015.

710 GAPHAZ: Assessment of glacier and permafrost hazards in Mountain Regions, in: Joint Standing Group  
711 on Glacier and Permafrost Hazards in High Mountains (GAPHAZ) of the International Association of  
712 Cryospheric Sciences (IACS) and the International Permafrost Association (IPA), edited by: Allen, S. K.,  
713 Frey, H., and Huggel, C., Zurich, Lima, available online at:  
714 [http://gaphaz.org/files/Assessment\\_Glacier\\_Permafrost\\_Hazards\\_Mountain\\_Regions.pdf](http://gaphaz.org/files/Assessment_Glacier_Permafrost_Hazards_Mountain_Regions.pdf), 2017.

715 GRASS Development Team: Geographic Resources Analysis Support System (GRASS) Software, Open  
716 Source Geospatial Foundation Project, <https://grass.osgeo.org>, last access: 4 February 2019.

717 Haeberli, W.: Frequency and characteristics of glacier floods in the Swiss Alps, *Ann. Glaciol.*, 4, 85–90,  
718 <https://doi.org/10.3189/S0260305500005280>, 1983.

719 Harrison, S., Kargel, J. S., Huggel, C., Reynolds, J., Shugar, D. H., Betts, R. A., Emmer, A., Glasser, N.,  
720 Haritashya, U. K., Klimeš, J., Reinhardt, L., Schaub, Y., Wilyshire, A., Regmi, D., and Vilímek, V.: Cli-  
721 mate change and the global pattern of moraine-dammed glacial lake outburst floods. *Cryosphere*, 12,  
722 1195–1209, <https://doi.org/10.5194/tc-12-1195-2018>, 2018.

723 Hewitt, K., and Liu, J.: Ice-dammed lakes and outburst floods, Karakoram Himalaya: historical perspec-  
724 tives on emerging threats, *Phys. Geogr.*, 31(6), 528–551, <https://doi.org/10.2747/0272-3646.31.6.528>,  
725 2010.

726 Hewitt, K.: Natural dams and outburst floods in the Karakorum Himalaya, in: *Hydrological aspects of*  
727 *alpine and high-mountain areas*, edited by: Glen, J. W., IAHS Publication, 138, 259–269, 1982.

728 Hofflinger, A., Somos-Valenzuela, M.A., and Vallejos-Romero, A.: Response time to flood events using a  
729 social vulnerability index (ReTSVI), *Nat. Hazards Earth Syst. Sci.*, 19, 251–267,  
730 <https://doi.org/10.5194/nhess-19-251-2019>, 2019.

731 Horizons: Horizons South America S.A.C.: Informe Técnico del Proyecto, Consultoría Para El Levan-  
732 tamiento Fotogramétrico Detallado De La Sub Cuenca Del Río Quillcay Y La Ciudad De Huaráz  
733 Para El Proyecto, Implementación de Medidas de Adaptación al Cambio Climático y Gestión de Ries-  
734 gos en la Subcuenca Quillcay (IMACC-QUILLCAY) – BID-MINAM (PE-T1168), Ministerio Del Ambi-  
735 ente A Travel Del Fonam – Administrador De Los Recursos Del BID, Lima, Peru, 2013.

736 Hubbard, B., Heald, A., Reynolds, J. M., Quincey, D., Richardson, S.D., Luyo, M.Z., Portilla, N.S., and  
737 Hambrey, M.J.: Impact of a rock avalanche on a moraine-dammed proglacial lake: Laguna Safuna Alta,  
738 Cordillera Blanca, Peru, *Earth Surf. Proc. Landforms*, 30(10), 1251–1264,  
739 <https://doi.org/10.1002/esp.1198>, 2005.

740 Huggel, C., Kääb, A., Haeberli, W., and Krummenacher, B.: Regional-scale GIS-models for assessment of  
741 hazards from glacier lake outbursts: evaluation and application in the Swiss Alps, *Nat. Hazards Earth*  
742 *Syst. Sci.*, 3, 647–662, <https://doi.org/10.5194/nhess-3-647-2003>, 2003.

743 Iturriaga, L.: Glacial and glacially conditioned lake types in the Cordillera Blanca, Peru: A spatiotem-  
744 poral conceptual approach, *Prog. Phys. Geogr.*, 38, 602–636, <https://doi.org/10.1177/0309133314546344>,  
745 2014.

746 Iverson, R. M.: The physics of debris flows, *Rev. Geophys.*, 35, 245–296,  
747 <https://doi.org/10.1029/97RG00426>, 1997.

748 Kafle, J., Pokhrel, P. R., Khattri, K. B., Kattel, P., Tuladhar, B. M., and Pudasaini, S. P.: Landslide-  
749 generated tsunami and particle transport in mountain lakes and reservoirs, *Ann. Glaciol.*, 57(71), 232–  
750 244, <https://doi.org/10.3189/2016AoG71A034>, 2016.

751 Kafle, J., Kattel, P., Mergili, M., Fischer, J.-T., and Pudasaini, S. P.: Dynamic response of submarine ob-  
752 stacles to two-phase landslide and tsunami impact on reservoirs. *Acta Mech.*, 230(9), 3143–3169,  
753 <https://doi.org/10.1007/s00707-019-02457-0>, 2019.

754 Kaser, G., and Georges, C.: A potential disaster in the Icy Andes: a regrettable blunder, technical report,  
755 University of Innsbruck, Austria, 2003.

756 Kattel, P., Khatri, K. B., Pokhrel, P. R., Kafle, J., Tuladhar, B. M., and Pudasaini, S. P.: Simulating gla-  
757 cial lake outburst floods with a two-phase mass flow model, *Ann. Glaciol.*, 57(71), 349–358,  
758 <https://doi.org/10.3189/2016AoG71A039>, 2016.

759 Kinzl, H., and Schneider, E.: *Cordillera Blanca (Perú)*, Universitäts-Verlag Wagner, Innsbruck, Austria,  
760 1950.

761 Klimeš, J., Novotný, J., Novotná, I., de Urries, B. J., Vilímek, V., Emmer, A., Strozzi, T., Kusák, M., Co-  
762 chachin, A., Hartvich, F., and Frey, H.: Landslides in moraines as triggers of glacial lake outburst floods:  
763 example from Palcacocha Lake (Cordillera Blanca, Peru), *Landslides*, 13(6), 1461–1477,  
764 <https://doi.org/10.1007/s10346-016-0724-4>, 2016.

765 McDougall, S., and Hungr, O.: A Model for the Analysis of Rapid Landslide Motion across Three-  
766 Dimensional Terrain, *Can. Geotech. J.*, 41, 1084–1097, <https://doi.org/10.1139/t04-052>, 2004.

767 Mergili, M., and Pudasaini, S. P.: r.avaflow – The open source mass flow simulation model,  
768 <https://www.avaflow.org/>, last access: 9 July 2019.

769 Mergili, M., and Schneider, J. F.: Regional-scale analysis of lake outburst hazards in the southwestern  
770 Pamir, Tajikistan, based on remote sensing and GIS, *Nat. Hazards Earth Syst. Sci.*, 11, 1447–1462,  
771 <https://doi.org/10.5194/nhess-11-1447-2011>, 2011.

772 Mergili, M., Schneider, D., Wormi, R., and Schneider, J.F.: Glacial Lake Outburst Floods (GLOFs): chal-  
773 lenges in prediction and modelling, in: *Proceedings of the 5th International Conference on Debris-Flow*  
774 *Hazards Mitigation: Mechanics, Prediction and Assessment*, Padova, June 14–17, 2011, edited by: Gene-  
775 vois, R., Hamilton, D. L., and Prestininzi, A., *Italian Journal of Engineering Geology and Environment –*  
776 *Book*, 973–982, 2011.

777 Mergili, M., Müller, J. P., and Schneider, J. F.: Spatio-temporal development of high-mountain lakes in  
778 the headwaters of the Amu Darya river (Central Asia), *Glob. Planet. Change*, 107, 13–24,  
779 <https://doi.org/10.1016/j.gloplacha.2013.04.001>, 2013.

780 Mergili, M., Fischer, J.-T., Krenn, J., and Pudasaini, S. P.: r.avaflow v1, an advanced open source compu-  
781 tational framework for the propagation and interaction of two-phase mass flows, *Geosci. Model Dev.*, 10,  
782 553–569, <https://doi.org/10.5194/gmd-10-553-2017>, 2017.

783 Mergili, M., Emmer, A., Juřicová, A., Cochachin, A., Fischer, J.-T., Huggel, C., and Pudasaini, S.P.: How  
784 well can we simulate complex hydro-geomorphic process chains? The 2012 multi-lake outburst flood in  
785 the Santa Cruz Valley (Cordillera Blanca, Perú), *Earth Surf. Process. Landf.*, 43(7), 1373–1389,  
786 <https://doi.org/10.1002/esp.4318>, 2018a.

787 Mergili, M., Frank, B., Fischer, J.-T., Huggel, C., and Pudasaini, S. P.: Computational experiments on the  
788 1962 and 1970 landslide events at Huascarán (Peru) with r.avaflow: Lessons learned for predictive mass  
789 flow simulations, *Geomorphology*, 322, 15–28, <https://doi.org/10.1016/j.geomorph.2018.08.032>, 2018b.

790 Mergili, M., Jaboyedoff, M., Pullarello, J., and Pudasaini, S. P.: Back-calculation of the 2017 Piz Cengalo-  
791 Bondo landslide cascade with r.avaflow, *Nat. Hazards Earth Syst. Sci. Discuss.*,  
792 <https://doi.org/10.5194/nhess-2019-204>, in review, 2019.

793 Nessimyahu, H., and Tadmor, E.: Non-oscillatory central differencing for hyperbolic conservation laws, *J.*  
794 *Comput. Phys.*, 87, 408–463, [https://doi.org/10.1016/0021-9991\(90\)90260-8](https://doi.org/10.1016/0021-9991(90)90260-8), 1990.

795 Ojeda, N.: Consolidacion laguna Palcacocha, ELECTROPERU S.A., Unidad de glaciologia y seguridad de  
796 lagunas, Huaráz, Peru, 1974.

797 Oppenheim, V.: Sobre las Lagunas de Huaráz, *Boletin de la Sociedad Geologica del Peru*, 19, 68–80, 1946.

798 Pitman, E.B., and Le, L.: A two-fluid model for avalanche and debris flows. *Philos. Trans. R. Soc. A*, 363,  
799 1573–1601, <https://doi.org/10.1098/rsta.2005.1596>, 2005.

800 Portocarrero, C.: Seminario desastres naturales – geologia, causes, efectos y prevenciones, ELEC-  
801 TROPERU S.A., Unidad de glaciologia y seguridad de lagunas, Huaráz, Peru, 1984.

802 Portocarrero, C.: The Glacial Lake Handbook: Reducing Risk from Dangerous Glacial Lakes in the Cor-  
803 dillera Blanca, Peru, Technical Report, United States Agency for International Development, Global  
804 Climate Change Office, Climate Change Resilient Development Project, Washington D.C., 2014.

805 Pudasaini, S. P.: A general two-phase debris flow model, *J. Geophys. Res. Earth Surf.*, 117, F03010,  
806 <https://doi.org/10.1029/2011JF002186>, 2012.

807 Pudasaini, S. P.: A full description of generalized drag in mixture mass flows, *Phys. Fluids*, submitted  
808 manuscript, 2019a.

809 Pudasaini, S. P.: A fully analytical model for virtual mass force in mixture flows, *Int. J. Multiph. Flow*,  
810 113, 142–152, <https://doi.org/10.1016/j.ijmultiphaseflow.2019.01.005>, 2019b.

811 Pudasaini, S. P., and Hutter, K.: Avalanche Dynamics: Dynamics of rapid flows of dense granular ava-  
812 lanches, Springer, 2007.

813 Pudasaini, S. P., and Krautblatter, M.: A two-phase mechanical model for rock-ice avalanches, *J. Ge-  
814 ophys. Res. Earth Surf.*, 119, <https://doi.org/10.1002/2014JF003183>, 2014.

815 Pudasaini, S. P., and Fischer, J.-T.: A mechanical model for phase-separation in debris flow,  
816 [arXiv:1610.03649](https://arxiv.org/abs/1610.03649), 2016a.

817 Pudasaini, S.P., and Fischer, J.-T.: A mechanical erosion model for two-phase mass flows,  
818 [arXiv:1610.01806](https://arxiv.org/abs/1610.01806), 2016b.

819 Pudasaini, S.P., and Mergili, M.: A Multi-Phase Mass Flow Model, *J. Geophys. Res. Earth Surf.*,  
820 JGRF21102, <https://doi.org/10.1029/2019JF005204>, 2019.

821 R Core Team: R: A Language and Environment for Statistical Computing, R Foundation for Statistical  
822 Computing, Vienna, Austria, <https://www.r-project.org/>, last access: 4 February 2019.

823 Reynolds, J. M.: Managing the risks of glacial flooding at hydro plants, *Hydro Rev. Worldwide*, 6(2), 18–  
824 22, 1998.

825 Reynolds, J. M., Dolecki, A., and Portocarrero, C.: The construction of a drainage tunnel as part of glacial  
826 lake hazard mitigation at Hualcán, Cordillera Blanca, Peru, in: Maund, J., and Eddleston, M. (eds.), Geo-  
827 hazards in engineering geology, Geological Society Engineering Group Special Publication, 15, 41–48,  
828 1998.

829 Richardson, S. D., and Reynolds, J. M.: An overview of glacial hazards in the Himalayas, *Quat. Int.*,  
830 65/66, 31–47, [https://doi.org/10.1016/S1040-6182\(99\)00035-X](https://doi.org/10.1016/S1040-6182(99)00035-X), 2000.

831 Rivas, D. S., Somos-Valenzuela, M. A., Hodges, B.R., and McKinney, D. C.: Predicting outflow induced  
832 by moraine failure in glacial lakes: the Lake Palcacocha case from an uncertainty perspective, *Nat. Haz-  
833 ards Earth Syst. Sci.*, 15, 1163–1179, <https://doi.org/10.5194/nhess-15-1163-2015>, 2015.

834 Sattar, A., Goswami, A., and Kulkarni, A. V.: Application of 1D and 2D hydrodynamic modeling to study  
835 glacial lake outburst flood (GLOF) and its impact on a hydropower station in Central Himalaya, *Nat.  
836 Hazards*, 97(2), 535–553, <https://doi.org/10.1007/s11069-019-03657-6>, 2019a.

837 Sattar, A., Goswami, A., and Kulkarni, A. V.: Hydrodynamic moraine-breach modeling and outburst  
838 flood routing-A hazard assessment of the South Lhonak lake, Sikkim, *Sci. Tot. Env.*, 668, 362–378,  
839 <https://doi.org/10.1016/j.scitotenv.2019.02.388>, 2019b.

840 Savage, S. B., and Hutter, K.: The motion of a finite mass of granular material down a rough incline, *J.  
841 Fluid Mech.*, 199, 177–215, <https://doi.org/10.1017/S0022112089000340>, 1989.

842 Schaub, Y., Huggel, C., and Cochachin, A.: Ice-avalanche scenario elaboration and uncertainty propaga-  
843 tion in numerical simulation of rock-/ice-avalanche-induced impact waves at Mount Hualcán and Lake  
844 513, Peru, *Landslides*, 13, 1445–1459, <https://doi.org/10.1007/s10346-015-0658-2>, 2016.

845 Schneider, D., Huggel, C., Cochachin, A., Guillén, S., and García, J.: Mapping hazards from glacier lake  
846 outburst floods based on modelling of process cascades at Lake 513, Carhuaz, Peru, *Adv. Geosci.*, 35,  
847 145–155, <https://doi.org/10.5194/adgeo-35-145-2014>, 2014.

848 Somos-Valenzuela, M. A., Chisolm, R. E., Rivas, D. S., Portocarrero, C., and McKinney, D. C.: Modeling  
849 a glacial lake outburst flood process chain: the case of Lake Palcacocha and Huaráz, Peru, *Hydrol. Earth  
850 Syst. Sci.*, 20, 2519–2543, <https://doi.org/10.5194/hess-20-2519-2016>, 2016.

851 Tai, Y. C., Noelle, S., Gray, J. M. N. T., and Hutter, K.: Shock-capturing and front-tracking methods for  
852 granular avalanches, *J. Comput. Phys.*, 175(1), 269–301, <https://doi.org/10.1006/jcph.2001.6946>, 2002.

853 Takahashi, T., Nakagawa, H., Harada, T., and Yamashiki, Y.: Routing debris flows with particle segrega-  
854 tion, *J. Hydraul. Res.*, 118, 1490–1507, [https://doi.org/10.1061/\(ASCE\)0733-9429\(1992\)118:11\(1490\)](https://doi.org/10.1061/(ASCE)0733-9429(1992)118:11(1490)),  
855 1992.

856 Turzewski, M. D., Huntington, K. W., and LeVeque, R. J.: The geomorphic impact of outburst floods:  
857 Integrating observations and numerical simulations of the 2000 Yigong flood, eastern Himalaya, *J. Ge-  
858 ophys. Res. Earth Surf.*, <https://doi.org/10.1029/2018JF004778>, 2019.

859 Vilímek, V., Zapata, M. L., Klimeš, J., Patzelt, Z., and Santillán, N.: Influence of glacial retreat on natural  
860 hazards of the Palcacocha Lake area, Peru, *Landslides*, 2(2), 107–115, [https://doi.org/10.1007/s10346-005-0052-6](https://doi.org/10.1007/s10346-<br/>861 005-0052-6), 2005.

862 Voellmy, A.: Über die Zerstörungskraft von Lawinen, Schweizerische Bauzeitung, 73, 159–162, 212–217,  
863 246–249, 280–285, 1955.

864 Walder, J. S., and O'Connor, J. E.: Methods for predicting peak discharge of floods caused by failure of  
865 natural and constructed earthen dams, Water Resour. Res., 33(10), 2337–2348,  
866 <https://doi.org/10.1029/97WR01616>, 1997.

867 Wegner, S. A.: Lo Que el Agua se Llevó: Consecuencias y Lecciones del Aluvión de Huaráz de 1941,  
868 Technical Note 7 of the series “Technical Notes on Climate Change”, Ministry of Environment, Lima,  
869 Peru, 2014.

870 Wang, Y., Hutter, K., and Pudasaini, S. P.: The Savage-Hutter theory: A system of partial differential  
871 equations for avalanche flows of snow, debris, and mud, ZAMM – J. Appl. Math. Mech., 84(8), 507–527,  
872 <https://doi.org/10.1002/zamm.200310123>, 2004.

873 Westoby, M. J., Glasser, N. F., Brasington, J., Hambrey, M. J., Quincey, D. J., and Reynolds, J. M.: Model-  
874 ling outburst floods from moraine-dammed glacial lakes, Earth-Sci. Rev., 134, 137–159,  
875 <https://doi.org/10.1016/j.earscirev.2014.03.009>, 2014.

876 Worni, R., Huggel, C., Clague, J. J., Schaub, Y., and Stoffel, M.: Coupling glacial lake impact, dam  
877 breach, and flood processes: A modeling perspective, Geomorphology, 224, 161–176,  
878 <https://doi.org/10.1016/j.geomorph.2014.06.031>, 2014.

879 Zapata, M. L.: Lagunas con obras de seguridad en la Cordillera Blanca, INGEOMIN, glaciología y seguri-  
880 dad de lagunas, Huaráz, Peru, 1978.

881 Zapata, M. L., Gómez, R. J. L., Santillán, N. P., Espinoza, H. V., and Huamaní, A.H.: Evaluacion del es-  
882 tado de los glaciares en la cabecera de la laguna Palcacocha, Informe tecnico, INRENA, INGEMMET,  
883 Huaráz, Peru, 2003.

884

885 **Tables**

886 Table 1. Characteristics of Lake Palcacocha (1941 and 2016) and Lake Jircacocha (1941), and changes due  
 887 to the 1941 GLOF. Topographic reconstruction according to field observations, historic photographs,  
 888 Vilímek et al. (2005), ANA (2016).

Parameter	Lake Palcacocha at 1941 GLOF	Lake Palcacocha 2016	Lake Jircacocha at 1941 GLOF
Lake level elevation (m a.s.l.)	4,610	4,563	~4,130
Surface area ( $10^3$ m $^2$ )	303	514	215
Lake volume ( $10^6$ m $^3$ )	12.9 <sup>1)</sup>	17.4	3.3
GLOF volume ( $10^6$ m $^3$ )	10.9 <sup>2)</sup>	–	3.3
Max. lake depth (m)	108 <sup>3)</sup>	71	33
Lowering of lake level (m)	47 <sup>2)</sup>	–	33

889 <sup>1)</sup> Reference values differ among sources: according to Vilímek et al. (2005), the volume of Lake Palcacocha  
 890 in 1941 was 9–11 million m $^3$ , whereas a reconstruction of ANA resulted in 13.1 million m $^3$ . In con-  
 891 trast, Vilímek et al. (2005) estimate a pre-failure volume of 4.8 million m $^3$  for Lake Jircacocha, whereas,  
 892 according to ANA, the volume was only 3.0 million m $^3$ .

893 <sup>2)</sup> Computed from the difference between the pre-1941 lake level and the modern lake level (before mit-  
 894 igation) of 4563 m. A reconstruction of ANA in 1948 resulted in a residual lake volume of approx.  
 895 100,000 m $^3$  and a residual depth of 17 m, both much smaller than derived through the reconstruction in  
 896 the present work. One of the reasons for this discrepancy might be the change of the glacier in the peri-  
 897 od 1941–1948.

898 <sup>3)</sup> This value is highly uncertain and might represent an overestimation: the maximum depth of the lake  
 899 strongly depends on the exact position of the glacier terminus, which was most likely located in an area  
 900 of increasing lake depth in 1941.

901

902 Table 2. Reference information used for back-calculation of the 1941 process chain.

Parameter	Value	Remarks	References
Impact area	4.3 km <sup>2</sup> <sup>1)</sup>	Mapped from post-event aerial images	Servicio Aerofotogramétrico Nacional
Breach volume – Palcacocha	2.0 million m <sup>3</sup>	Comparison of pre- and post-event DTMs	Topographic reconstruction ( Sect. 4)
Breach depth – Palcacocha	76 m	Elevation change at reference point R1 (Fig. 4)	Topographic reconstruction (Sect. 4)
Breach volume – Jircacocha	2.8 million m <sup>3</sup>	Comparison of pre- and post-event DTMs	Topographic reconstruction (Sect. 4)
Material entrained upstream from Lake Jircacocha	1.0 million m <sup>3</sup>	Maximum, value might be much lower	Topographic reconstruction (Sect. 4)
Material entrained downstream from Lake Jircacocha	3.1 million m <sup>3</sup>	Maximum, value might be much lower	Topographic reconstruction ( Sect. 4)
Material entrained in promontory	7.3 million m <sup>3</sup>	Maximum, value might be much lower	Topographic reconstruction (Sect. 4)
Maximum depth of entrainment in promontory	50 m	Rough estimate	Somos-Valenzuela et al. (2016)
Material arriving at Huaráz	4–6 million m <sup>3</sup>		Kaser and Georges (2003)

903 <sup>1)</sup> Includes the surface of Lake Palcacocha

904

905 Table 3. Key model parameters applied to the simulations in the present work. Where three values are  
 906 given, the first value applies to the glacier, the second value to the remaining area upstream of the dam  
 907 of Lake Jircacocha, and the third value to the area downstream of the dam of Lake Jircacocha.

Symbol	Parameter	Unit	Value
$\rho_s$	Solid material density (grain density)	$\text{kg m}^{-3}$	2,700
$\rho_f$	Fluid material density	$\text{kg m}^{-3}$	1,000 <sup>1)</sup>
$\varphi$	Internal friction angle	Degree	28
$\delta$	Basal friction angle	Degree	6, 12, 7
$\nu$	Kinematic viscosity of fluid	$\text{m}^2 \text{s}^{-1}$	~0
$\tau_y$	Yield strength of fluid	Pa	0 <sup>2)</sup>
$C_{AD}$	Ambient drag coefficient	—	0.02, 0.005, 0.005
$C_{FF}$	Fluid friction coefficient	—	0.001, 0.004, 0.004
$C_E$	Entrainment coefficient	—	$10^{-6.75}$ <sup>3)</sup> , $10^{-7.15}$ <sup>4)</sup>

908 <sup>1)</sup> The fluid material density is set to 1,100  $\text{kg m}^{-3}$  in Scenario AX.

909 <sup>2)</sup> The yield strength of the fluid phase is set to 5 Pa in Scenario AX.

910 <sup>3)</sup> This value applies to the dam of Lake Palcacocha.

911 <sup>4)</sup> This value applies to all other areas.

913 Table 4. Empirical relationships for the peak discharge in case of breach of moraine and landslide dams  
 914 (Walder and O'Connor, 1997), and the peak discharges estimated for Lake Palcacocha and Lake Jircaco-  
 915 cha.  $q_p$  = peak discharge ( $\text{m}^3 \text{s}^{-1}$ ),  $V$  = total volume of water passing through the breach ( $\text{m}^3$ );  $D$  = drop of  
 916 lake level (m); REG = regression; ENV = envelope. The values of  $V$  and  $D$  for the two lakes are summa-  
 917 rized in Table 1. See also Rivas et al. (2015).

Moraine	$a_{\text{REG}}$	$a_{\text{ENV}}$	$b$	$q_p$ Palcacocha REG ( $\text{m}^3 \text{s}^{-1}$ )	$q_p$ Palcacocha ENV ( $\text{m}^3 \text{s}^{-1}$ )
$q_p = a \cdot V^b$	0.045	0.22	0.66	2,231	10,905
$q_p = a \cdot D^b$	60.3	610	0.84	1,531	15,484
$q_p = a \cdot (V \cdot D)^b$	0.19	1.1	0.47	2,560	14,819
Landslide	$a_{\text{REG}}$	$a_{\text{ENV}}$	$b$	$q_p$ Jircacocha REG ( $\text{m}^3 \text{s}^{-1}$ )	$q_p$ Jircacocha ENV ( $\text{m}^3 \text{s}^{-1}$ )
$q_p = a \cdot V^b$	1.6	46	0.46	1,638	47,101
$q_p = a \cdot D^b$	6.7	200	1.73	2,839	84,734
$q_p = a \cdot (V \cdot D)^b$	0.99	25	0.4	1,662	41,973

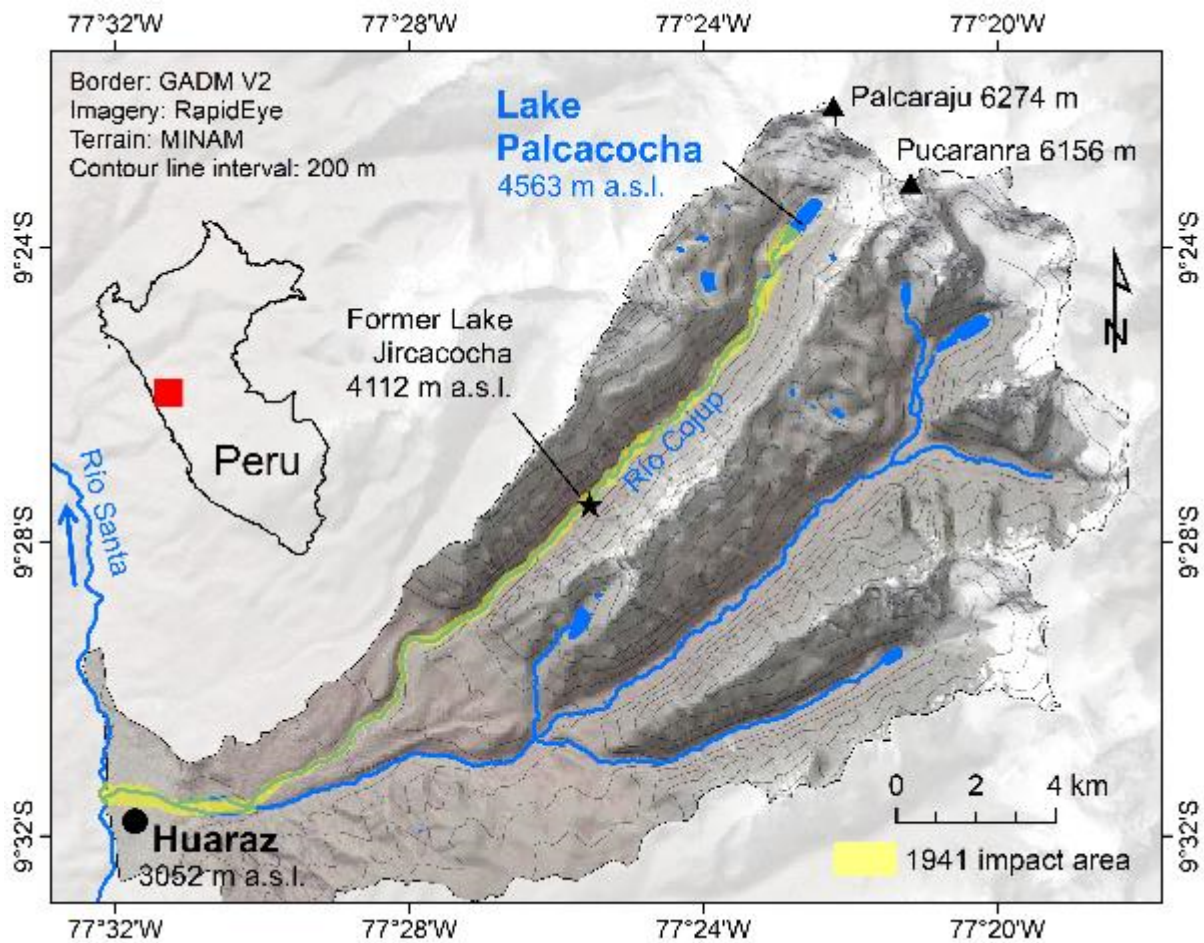
918

919 Table 5. Summary of the key results obtained with the computational experiments A–C. Refer to Ta-  
 920 bles 1 and 2 for the volumes involved, and to Table 4 for empirically expected peak discharges. Note that  
 921 all entrained volumes are composed of 80% of solid and 20% of fluid material in terms of volume.

Scenario	A	AX	B	C
Description	Overtopping	Overtopping	Impact wave	Dam collapse
Entrained volume Lake Palcacocha dam (m <sup>3</sup> )	1.5 million	1.4 million	2.7 million	–
Fluid peak discharge at outlet of Lake Palcacocha (m <sup>3</sup> s <sup>-1</sup> )	19,000	8,200	17,000 <sup>1)</sup>	38,000
Entrained volume Lake Jircacocha dam (m <sup>3</sup> )	2.2 million	2.0 million	2.2 million	2.2 million
Fluid peak discharge at outlet of Lake Jircacocha (m <sup>3</sup> s <sup>-1</sup> )	14,700	7,600	15,000	15,400
Material entrained upstream from Lake Jircacocha (m <sup>3</sup> )	0.7 million	0.7 million	0.7 million	0.7 million
Material entrained downstream from Lake Jircacocha (m <sup>3</sup> )	1.5 million	1.3 million	1.5 million	1.5 million
Material entrained in promontory (m <sup>3</sup> )	5.3 million	5.3 million	5.3 million	5.3 million
Travel time to Huaráz (s) Start (Peak)	2,760 (3,660)	4,200 (6,480)	3,060 (4,080)	2,160 (3,060)
Solid delivered to Huaráz (m <sup>3</sup> )	2.5 million	2.6 million	2.5 million	2.7 million

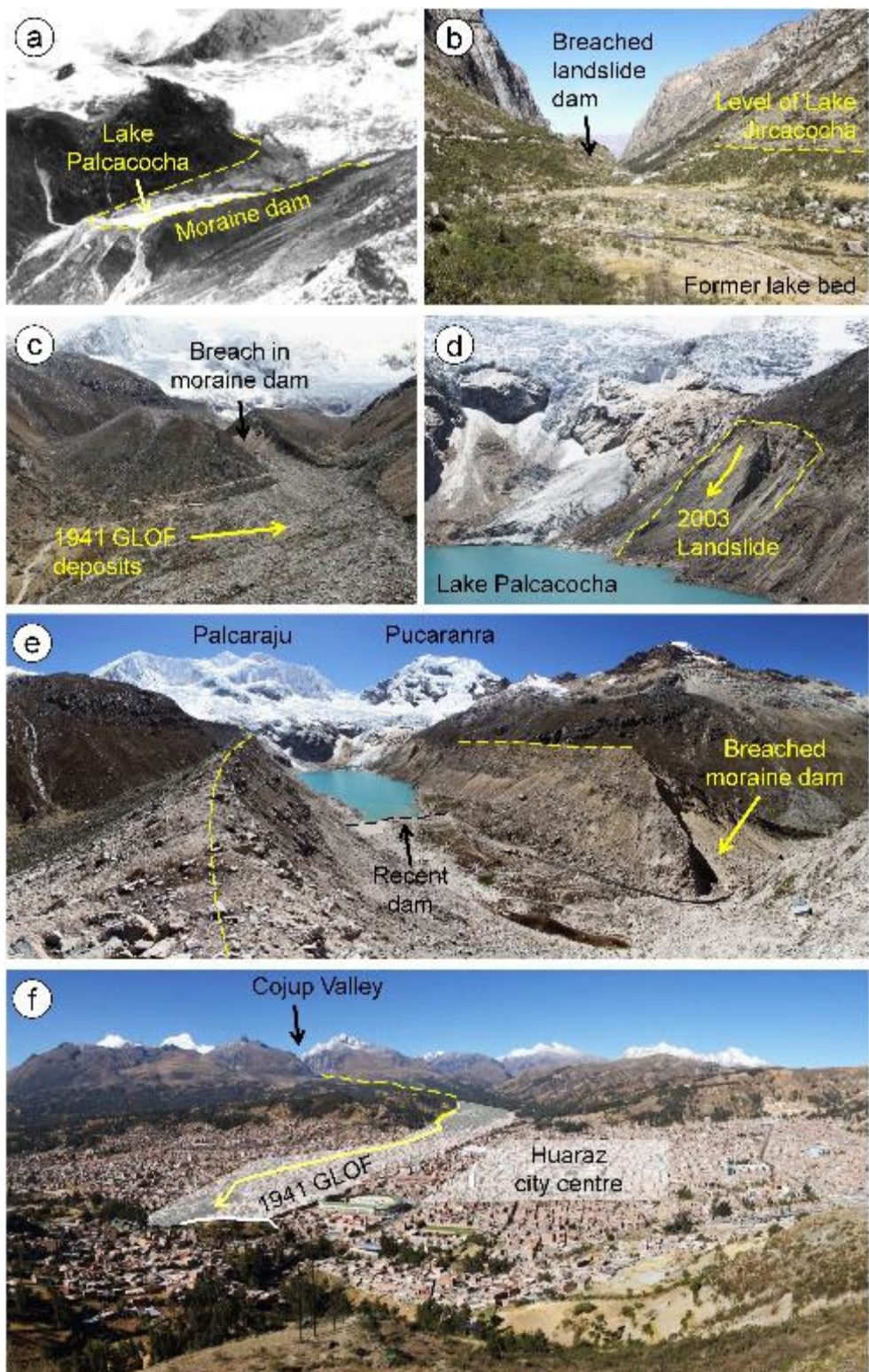
922 <sup>1)</sup> Peak of initial overtopping as response to the impact wave: 7,000 m<sup>3</sup> s<sup>-1</sup>

923 **Figures**



924  
925 Fig. 1. Location and main geographic features of the Quilcay catchment with Lake Palcacocha and the  
926 former Lake Jircacocha.

927

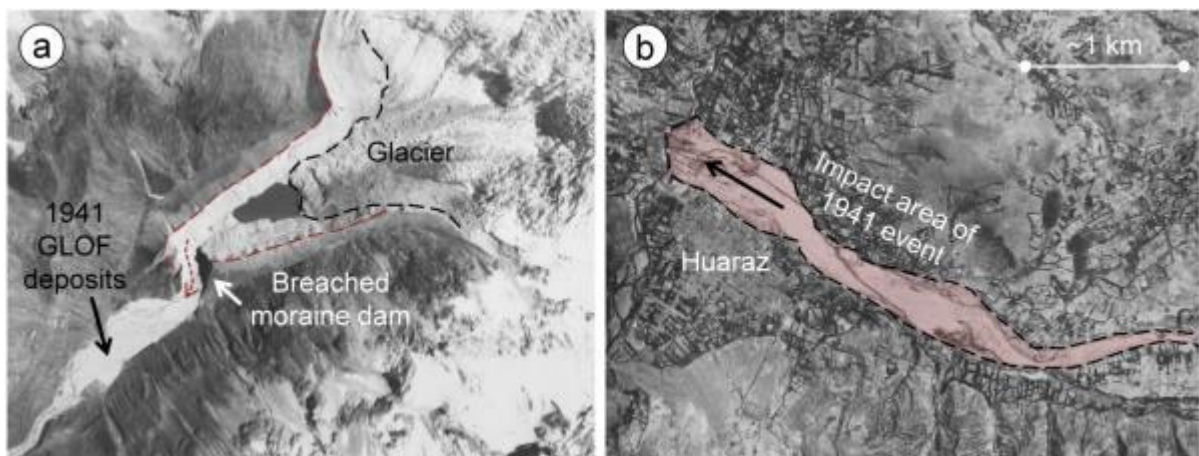


928

929 Fig. 2. The Quilcay catchment from Lake Palcacocha down to Huaráz. (a) Lake Palcacocha in 1939, two  
 930 years prior to the 1941 event. (b) The site of former Lake Jircacocha with the breached landslide dam  
 931 and the former lake level. (c) Breached moraine dam and 1941 GLOF deposits, seen from downstream.  
 932 (d) Left lateral moraine of Lake Palcacocha with landslide area of 2003. (e) Panoramic view of Lake Pal-  
 933 cacocha, with the breach in the moraine dam and the modern lake impounded by a smaller terminal  
 934 moraine and two artificial dams. (f) Panoramic view of Huaráz with city centre and approximate impact  
 935 area of the 1941 event. Note that a small part of the lowermost portion of the impact area is hidden be-

936 hind a hillslope. Photos: (a) Hans Kinzl, 1939 (Kinzl and Schneider, 1950); (b) Martin Mergili, July 2017;  
937 (c) Gisela Eberhard, July 2018; (d)–(f): Martin Mergili, July 2017.

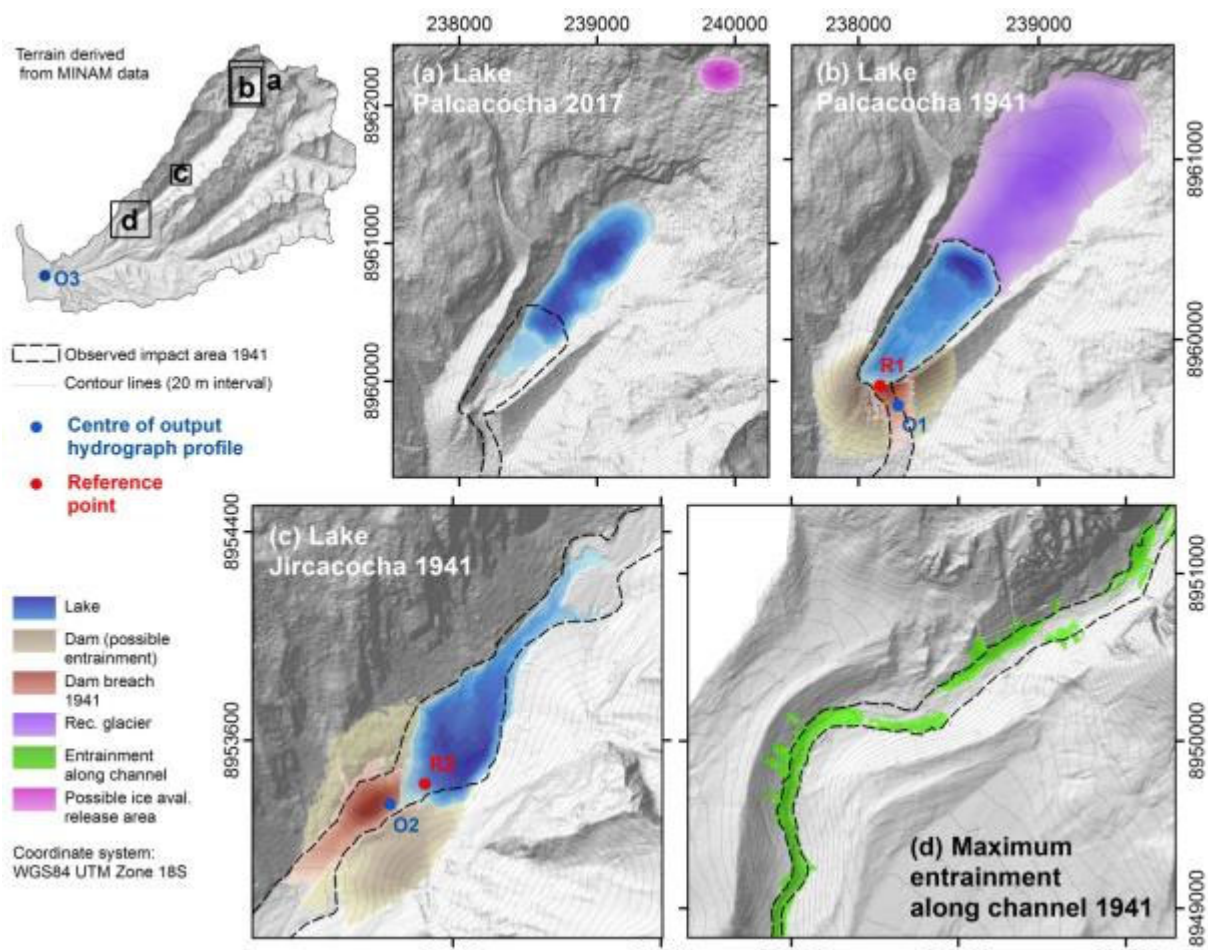
938



939

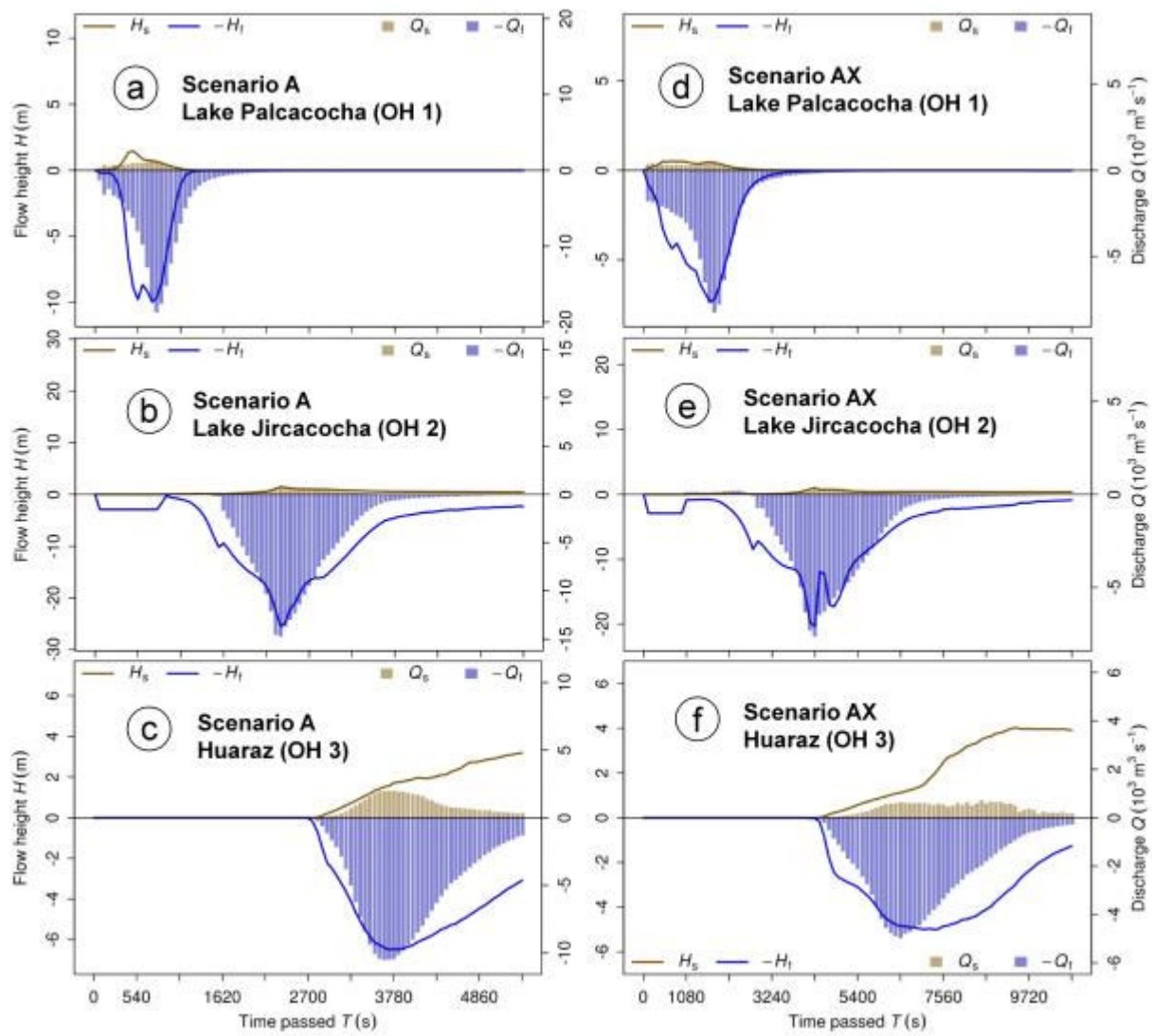
940 Fig. 3. Situation in 1948, seven years after the 1941 event. (a) Residual Lake Palcacocha, and traces of the  
941 1941 event. (b) Huaráz with the impact area of the 1941 event. Imagery source: Servicio Aerofoto-  
942 gramétrico Nacional, Perú.

943



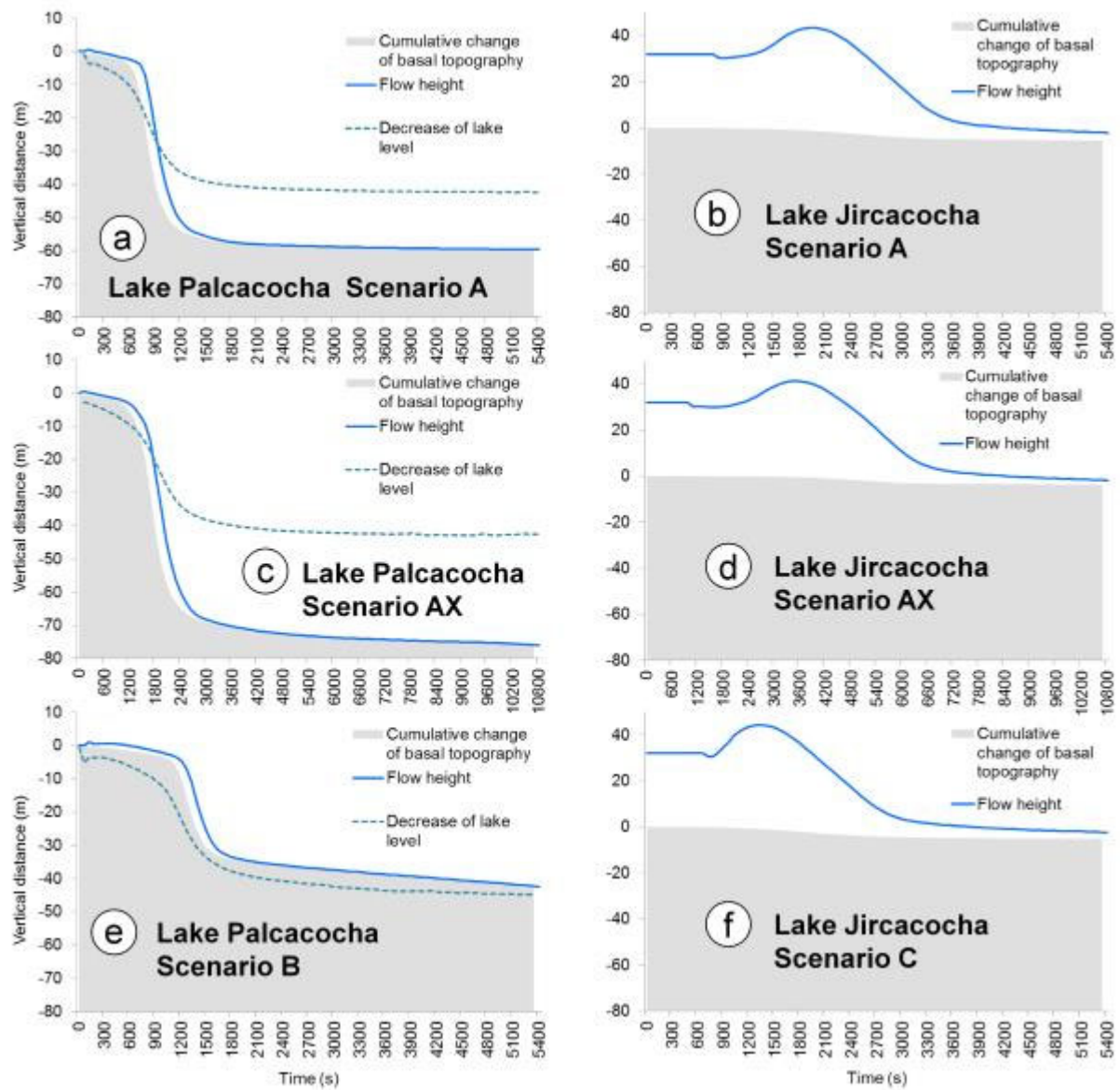
944  
945 Fig. 4. Reconstruction of lakes and topography. (a) Lake Palcacocha in 2017. (b) Lake Palcacocha before  
946 the 1941 event. (c) Lake Jircacocha before the 1941 event. (d) Part of the promontory section of the  
947 Cojup Valley, with lowering of the valley bottom by up to 50 m. The possible rock avalanche release  
948 area is shown in (a) for clarity, but is applied to the 1941 situation.

949



950  
951 Fig. 5. Hydrographs of moraine dam failure of Lake Palcacocha (a, d), landslide dam failure of Lake Jircacocha (b, e), and the flow entering the urban area of Huaráz (c, f) for the scenarios A and AX. Note that,  
952 for clarity, fluid flow heights and discharges are plotted in negative direction.  
953

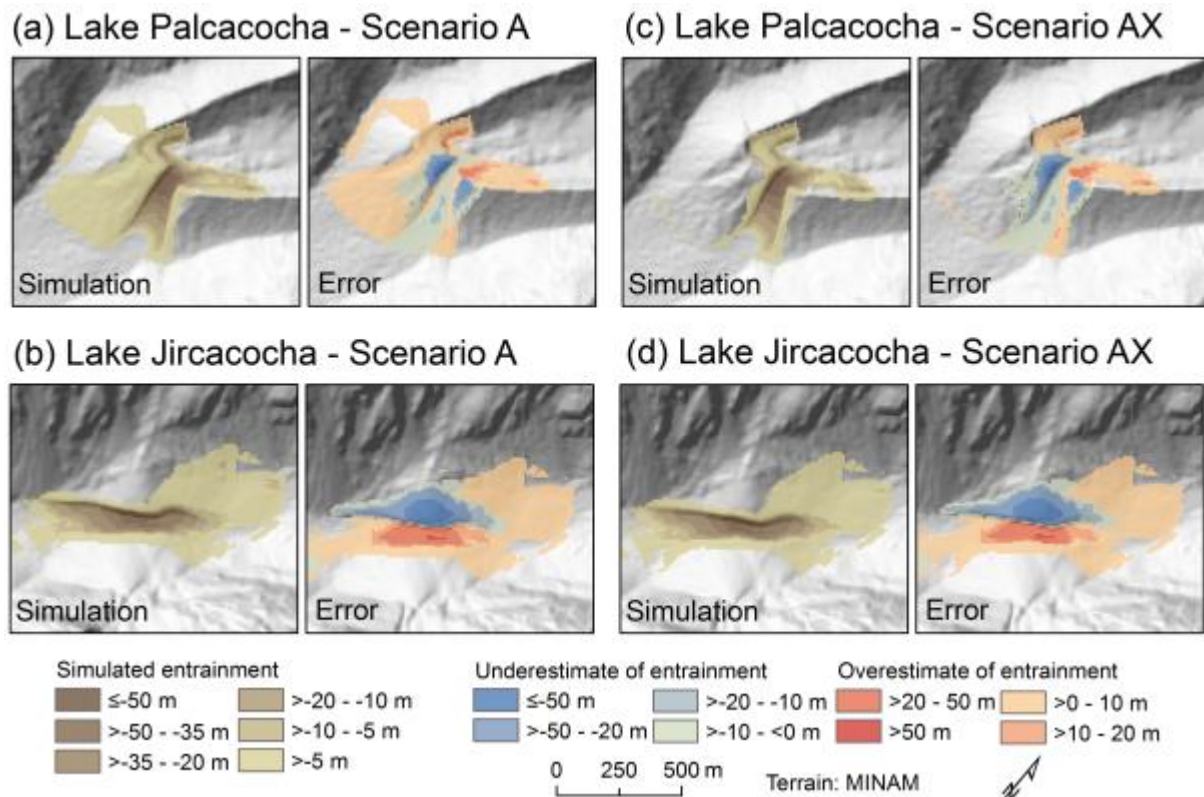
954



955

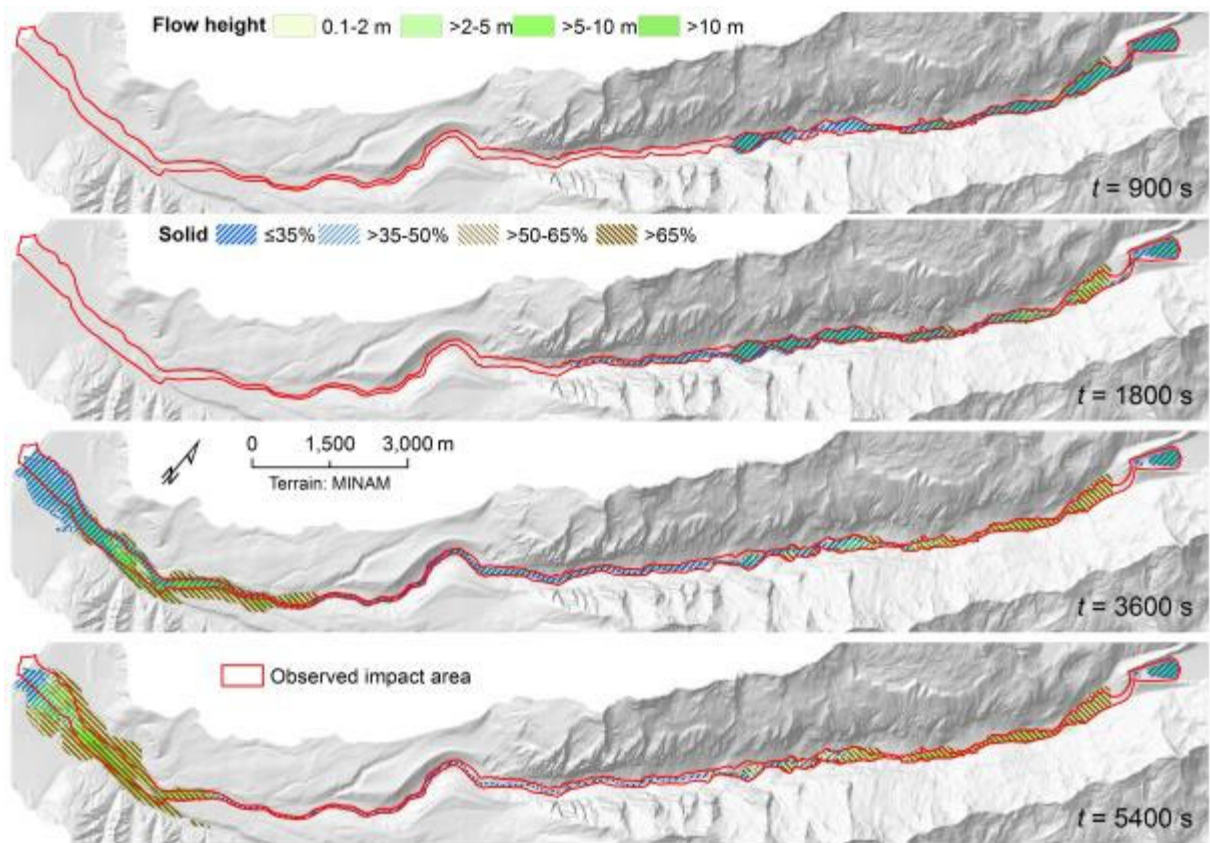
956 Fig. 6. Evolution of flow height and basal topography at the outlets of Lake Palcacocha (reference point  
 957 R1 in Fig. 4b), and Lake Jircacocha (reference point R2 in Fig. 4c). The reference points are placed in a  
 958 way to best represent the evolution of the breach in the dam for Lake Palcacocha, and the evolution of  
 959 the impact wave for Lake Jircacocha. Additionally, the evolution of the lake level is shown for Lake Pal-  
 960 cacocha. Note that the result for Scenario B is only displayed for Lake Palcacocha (e), whereas the result  
 961 for Scenario C is only illustrated for Lake Jircacocha (f). The vertical distance displayed on the y axis  
 962 refers to the terrain height or the lake level at the start of the simulation, respectively, whereby the flow  
 963 height is imposed onto the topography. In Scenario B, the initial impact wave at the dam of Lake Palca-  
 964 cocha is only poorly represented due to the low temporal resolution of the simulation, and due to blur-  
 965 ring by numerical effects (e).

966



967  
968 Fig. 7. Simulated versus reconstructed entrainment patterns for the scenarios A and AX. The total en-  
969 trained height and the difference between simulated and reconstructed entrainment (error) are shown.  
970 (a) Lake Palcacocha, Scenario A. (b) Lake Jircacocha, Scenario A. (c) Lake Palcacocha, Scenario AX.  
971 (d) Lake Jircacocha, Scenario AX.

972

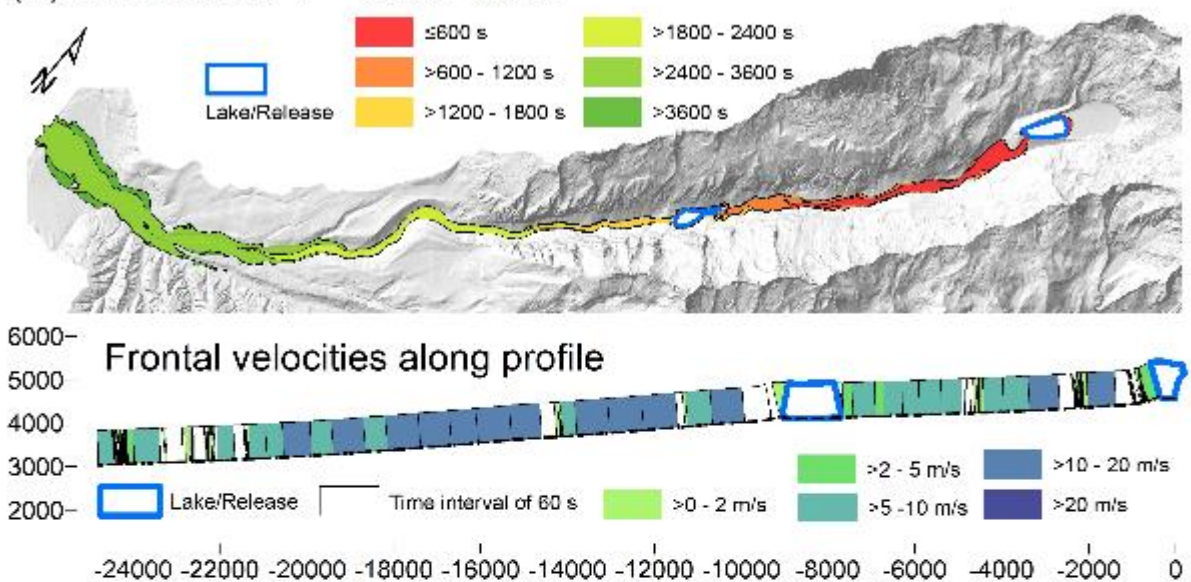


973  
974

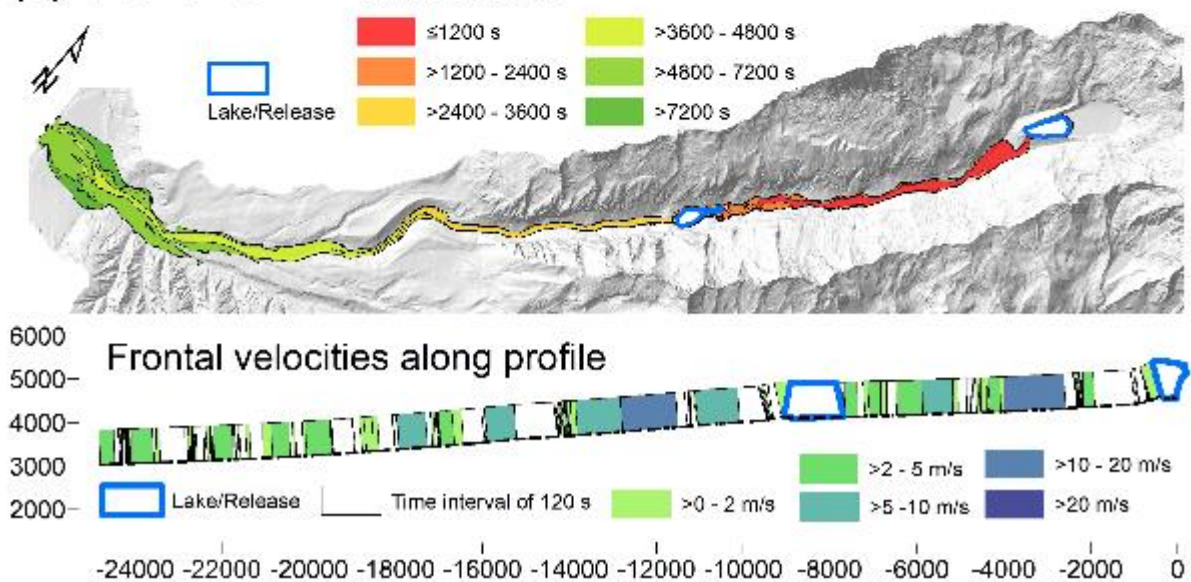
Fig. 8. Evolution of the flow in space and time (Scenario A).

975

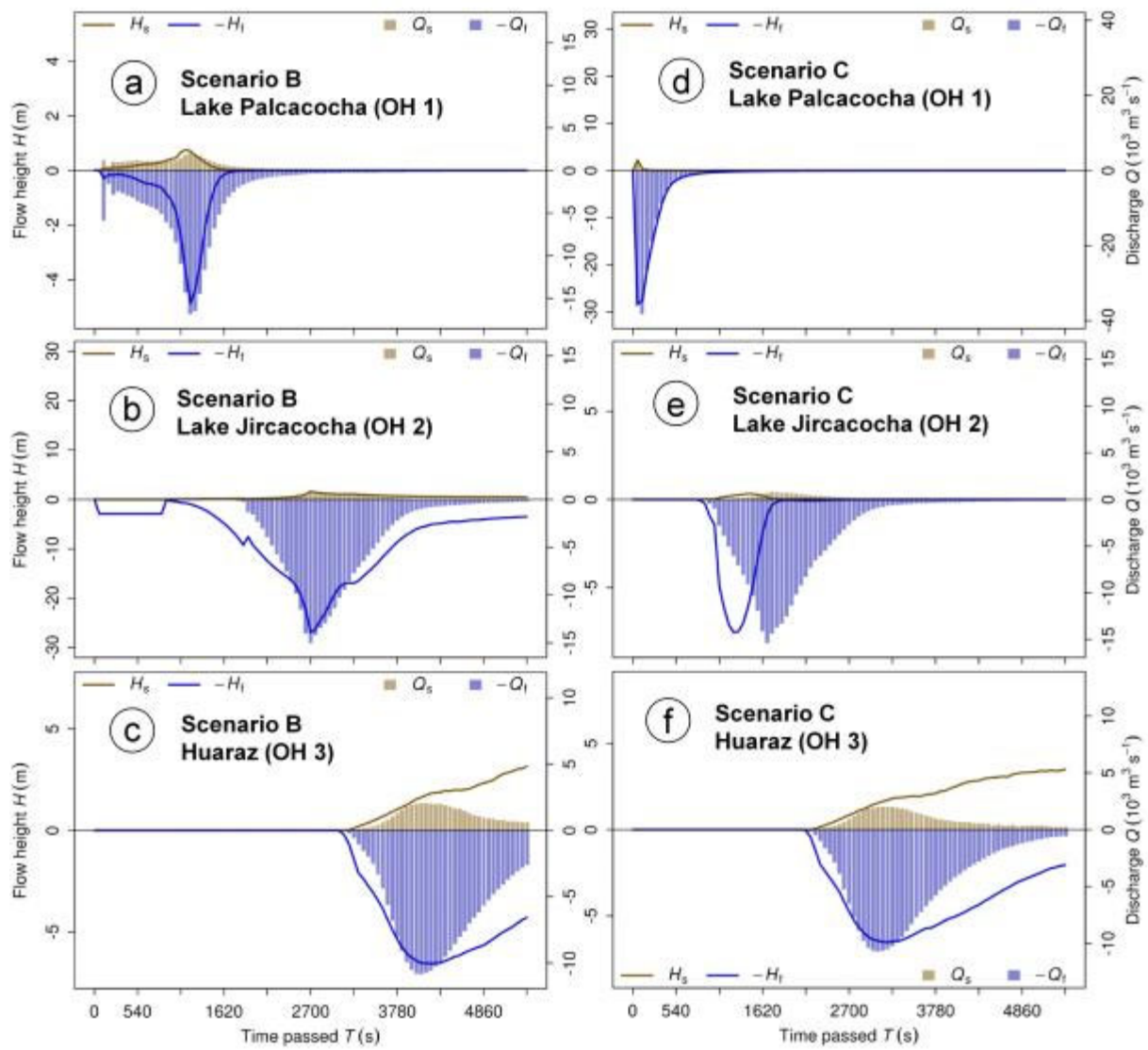
976 (a) Scenario A Travel times



978 (b) Scenario AX Travel times



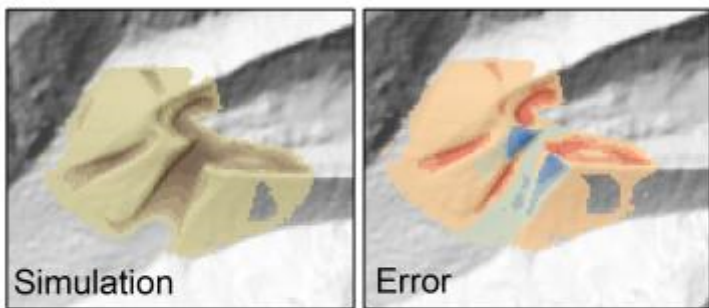
976 Fig. 9. Travel times and frontal velocities for the scenarios (a) A and (b) AX. Void fields in the profile  
977 graph refer to areas without clearly defined flow front.



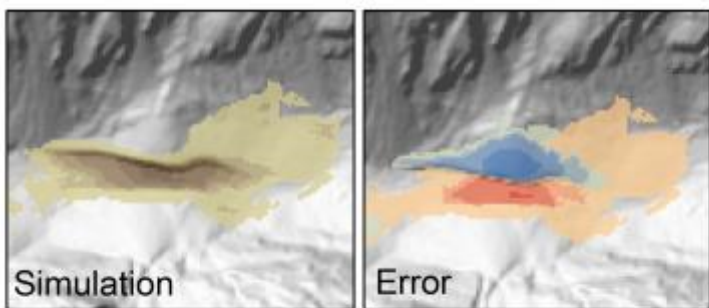
980  
981 Fig. 10. Hydrographs of moraine dam failure of Lake Palcacocha (a, d), landslide dam failure of Lake  
982 Jircacocha (b, e), and the flow entering the urban area of Huaráz (c, f) for the scenarios B and C. Note  
983 that, for clarity, fluid flow heights and discharges are plotted in negative direction.

984

### (a) Lake Palcacocha - Scenario B



### (b) Lake Jircacocha - Scenario B



Simulated entrainment

- $\leq -50$  m
- $> -50 - -35$  m
- $> -35 - -20$  m
- $> -20 - -10$  m
- $> -10 - -5$  m
- $> -5$  m

Overestimate of entrainment

- $> 20 - 50$  m
- $> 50$  m
- $> 0 - 10$  m
- $> 10 - 20$  m

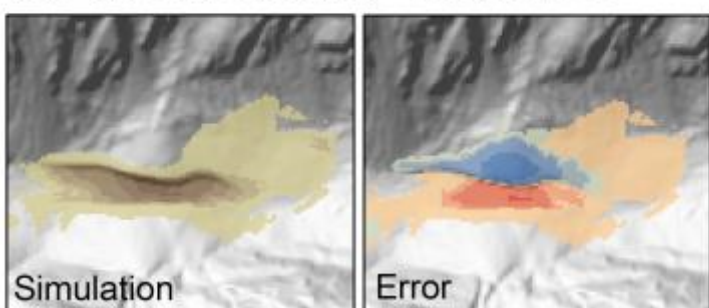
Underestimate of entrainment

- $\leq -50$  m
- $> -50 - -20$  m
- $> -20 - -10$  m
- $> -10 - <0$  m

0 250 500 m

Terrain: MINAM

### (c) Lake Jircacocha - Scenario C



985

986

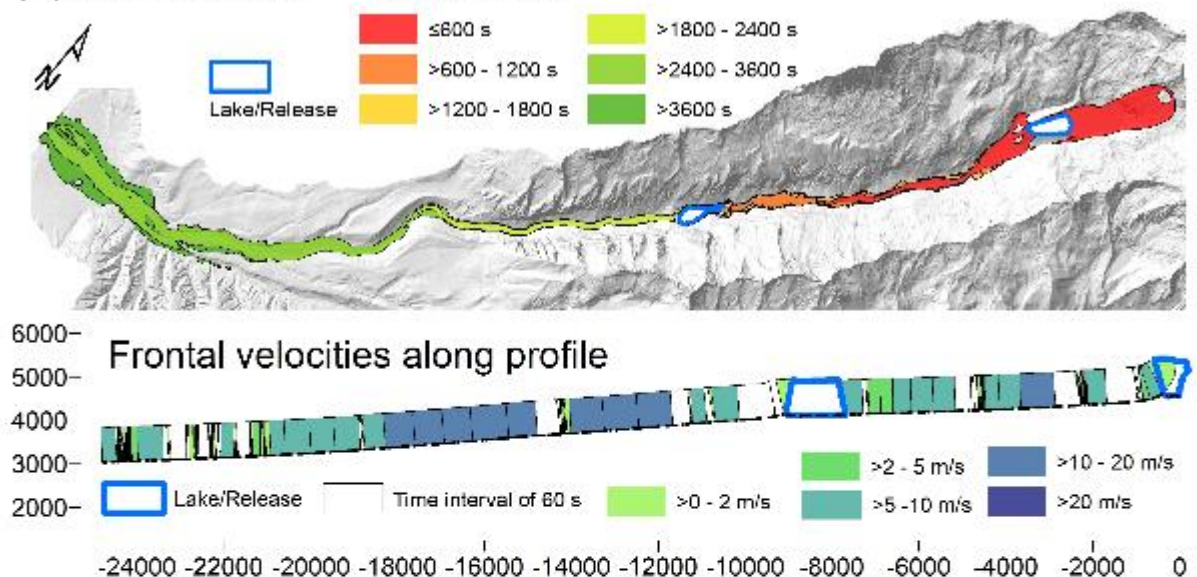
987

988

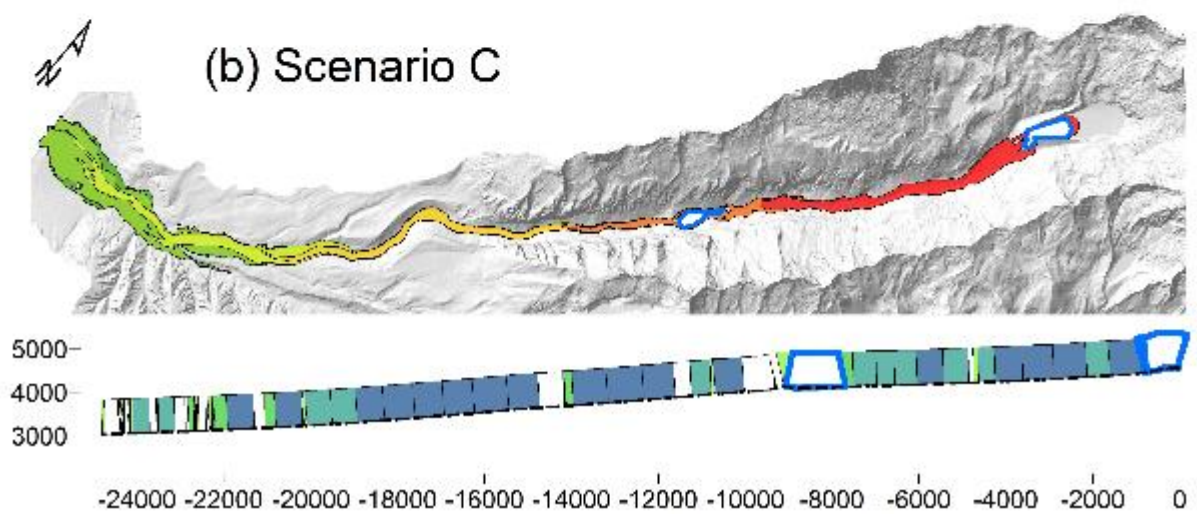
989

Fig. 11. Simulated versus reconstructed entrainment patterns for the scenarios B and C. The total entrained height and the difference between simulated and reconstructed entrainment (error) are shown. (a) Lake Palcacocha, Scenario B. (b) Lake Jircacocha, Scenario B. (c) Lake Jircacocha, Scenario C.

990 (a) Scenario B Travel times



992 (b) Scenario C



990 Fig. 12. Travel times and frontal velocities for the scenarios (a) B and (b) C. Note that the legend of (a)  
991 also applies to (b). Void fields in the profile graph refer to areas without clearly defined flow front.